

# TabPFN: One Model to Rule Them All?

Qiong Zhang<sup>1</sup>, Yan Shuo Tan<sup>1</sup>, Qinglong Tian<sup>1</sup>, and Pengfei Li

*Abstract.* Hollmann et al. (*Nature* **637** (2025) 319–326) recently introduced TabPFN, a transformer-based deep learning model for regression and classification on tabular data, which they claim “outperforms all previous methods on datasets with up to 10,000 samples by a wide margin, using substantially less training time.” Furthermore, they have called TabPFN a “foundation model” for tabular data, as it can support “data generation, density estimation, learning reusable embeddings and fine-tuning”. In this paper, we provide a tailored explanation of how TabPFN works for a statistics audience, by emphasizing its interpretation as approximate Bayesian inference. We then explore the significance of TabPFN to the field of statistics: We show that an out-of-the-box application of TabPFN can sometimes outperform specialized state-of-the-art methods for semi-supervised parameter estimation, prediction under covariate shift, and heterogeneous treatment effect estimation. As a partial explanation for the predictive effectiveness of TabPFN, we show that it can simultaneously adapt to both nonparametric structure and parametric structure, for instance, sometimes outperforming LASSO even when assumptions are correctly specified. All experiments can be reproduced using the code provided at [https://github.com/qinglong-tian/tapfn\\_study](https://github.com/qinglong-tian/tapfn_study).

*Key words and phrases:* Foundation models, in-context learning, meta-learning, tabular data, transformers.

## 1. INTRODUCTION

Deep learning has achieved remarkable success in modeling unstructured data types such as text and images. However, for tabular data—arguably the most prevalent and consequential data type across science—ensemble tree methods have remained the gold standard predictive modeling strategy, consistently outperforming even deep learning on benchmark datasets [11, 19, 24, 40]. This long-held wisdom has now been challenged by Hollmann et al. [30], who introduced a deep learning method for tabular data,

---

*Qiong Zhang is Assistant Professor, Institute of Statistics & Big Data, Renmin University of China, China (e-mail: [qiong.zhang@ruc.edu.cn](mailto:qiong.zhang@ruc.edu.cn)). Yan Shuo Tan is Assistant Professor, Department of Statistics & Data Science, National University of Singapore, Singapore (e-mail: [yanshuo@nus.edu.sg](mailto:yanshuo@nus.edu.sg)). Qinglong Tian is Assistant Professor, Department of Statistics & Actuarial Science, University of Waterloo, Canada (e-mail: [qinglong.tian@uwaterloo.ca](mailto:qinglong.tian@uwaterloo.ca)). Pengfei Li is Professor, Department of Statistics & Actuarial Science, University of Waterloo, Canada (e-mail: [pengfei.li@uwaterloo.ca](mailto:pengfei.li@uwaterloo.ca)).*

<sup>1</sup>Co-first author.

called *TabPFN*<sup>1</sup>, which they claimed “outperforms all previous methods on datasets with up to 10,000 samples by a wide margin, using substantially less training time.” As evidence, they showed that TabPFN significantly outperforms random forests, XGBoost, LightGBM, and CatBoost on 50+ benchmark classification and regression datasets.

Beyond its impressive predictive accuracy, TabPFN is claimed to be robust to outliers and missing data, and automatically estimates predictive distributions, thereby providing uncertainty quantification. Furthermore, it is claimed to support “data generation, density estimation, learning reusable embeddings and fine-tuning”. Because of this wide range of capabilities, Hollmann et al. [30] call TabPFN a “tabular foundation model” [52], appropriating a term that has been used to describe the transformative role played

---

<sup>1</sup>The version of the TabPFN model used in our study is the one introduced by Hollmann et al. [30], referred to there as TabPFNv2. While our paper was undergoing revision, the developers released an updated model, TabPFN-2.5 [25]. For consistency, all experiments and discussion in this paper are based on TabPFNv2.

by large language models (LLMs) [7] in natural language processing. TabPFN shares other similarities with LLMs: It makes use of the same type of deep learning architecture (transformers) [53] and the same learning paradigm (in-context learning) [9], which differs fundamentally from traditional statistical and machine learning approaches.

Our goal in this paper is not to further test the claims of Hollmann et al. [30], which have now been further validated on other benchmarks and by other sources (see for instance Erickson et al. [18]). Instead, we aim to provide an explanation of how TabPFN works that is tailored to a statistics audience (Section 2) and, more importantly, to explore the significance of TabPFN to the field of statistics. Towards this goal, we first demonstrate the utility of TabPFN in handling three currently researched estimation problems, namely semi-supervised parameter estimation (Section 3.1), heterogeneous treatment effects estimation (Section 3.2), and prediction under covariate shift (Section 3.3). For each problem, we compare a simple out-of-the-box application of TabPFN to a “state-of-the-art” method proposed by a selected paper recently published at a top statistics journal. Using the same simulation set-up described by the paper, augmented with further comparisons on real datasets, we show that *TabPFN often achieves better results than the comparator method*.

In addition, we investigate how the statistical principle of adaptivity [16] can provide a partial explanation for the predictive effectiveness of TabPFN. In classical nonparametric statistics, adaptivity refers to a procedure’s ability to automatically adjust to unknown aspects of the data-generating process, such as smoothness, sparsity, or latent structure, achieving optimal rates without relying on these properties being specified in advance. In Section 4, we perform numerical experiments suggesting that TabPFN, without any hyperparameter tuning, can simultaneously adapt to both parametric and nonparametric structure: It is competitive with and sometimes even outperforms parametric methods (e.g., LASSO and linear discriminant analysis) even in settings where the parametric assumptions are correct. At the same time, it outperforms local averaging and smoothing methods in misspecified settings—for example, classification problems with substantial label noise. Such adaptivity properties are beyond the reach of ensemble tree methods and other previous machine learning or nonparametric methods.

While TabPFN is not a perfect model, its capabilities indicate that “in-context learning” with a “foundation model” could become a powerful alternative to

conventional statistical methodologies across a variety of tasks. This emerging paradigm appears sufficiently promising to merit serious consideration alongside more established approaches. We define these terms and elaborate on their implications in Section 5, where we also discuss avenues for statisticians to guide and influence the field’s development.

## 2. AN OVERVIEW OF TABPFN

TabPFN makes use of *in-context learning* (ICL), which is a new learning paradigm that differs from the standard statistical learning approach to regression and classification and has gathered significant interest in the machine learning community. The meaning of ICL has changed over time. In TabPFN, ICL takes the form of approximate Bayesian inference; we elaborate on this perspective below and defer a discussion on the historical development of ICL to Section 5.

The **first key idea** of TabPFN is to approximate posterior predictive distributions (PPD) using a transformer model, which is the same deep learning architecture that powers LLMs. More precisely, let  $\Pi$  denote the space of joint distributions on covariate-label pairs  $(X, Y)$  and let  $n$  be a fixed sample size. Let  $p$  be a prior on  $\Pi$  and an observed training data  $\mathcal{D} = \{(X_i, Y_i)\}_{i=1}^n$  is drawn independently identically distributed (IID) from some fixed distribution  $\pi^* \in \Pi$ , let  $p(\pi|\mathcal{D})$  denote the posterior on  $\Pi$  given  $\mathcal{D}$ . With slight abuse of notation, the posterior predictive distribution (PPD) for  $Y_{n+1}$  given  $X_{n+1} = x$  is defined as

$$p(y|x, \mathcal{D}) = \int_{\Pi} \pi(y|x)p(\pi|\mathcal{D})d\pi.$$

The TabPFN transformer  $M$  is trained to approximate the mapping  $(\mathcal{D}, x) \mapsto p(y|x, \mathcal{D})$ . Müller et al. [37], who developed this approach, called the resulting model a *prior-fitted network* (PFN).

Approximating the PPD of a Bayesian regression or classification model is far from a new idea. Indeed, the popular Bayesian Additive Regression Trees (BART) algorithm does the same job via Markov chain Monte Carlo (MCMC) [13]. The novelty of the PFN approach is that while previous approaches (MCMC, variational inference, likelihood-free inference, etc.) attempt to approximate the map  $x \mapsto p(y|x, \mathcal{D})$  for a fixed training dataset  $\mathcal{D}$ , PFN tries to approximate the map jointly over  $x$  and  $\mathcal{D}$ . It has the computational benefit of amortizing computation, which is the basis of the “substantially less training time” claim by Hollmann et al. [30] regarding TabPFN.<sup>2</sup> Such an approximation

<sup>2</sup>Similar ideas have been explored in the variational inference community under the name of *Neural Processes* (NP) [23].

may also yield statistical benefits via implicit regularization that are not yet fully understood.

The **second key idea** of TabPFN is its choice of prior on the space of joint distribution  $\Pi$ . The large number of parameters of a transformer model ( $\approx 7M$  in the case of TabPFN) means that it could potentially approximate PPDs defined in terms of complicated priors. TabPFN chooses to define its prior in terms of structural causal models (SCMs) [41]. An SCM defines a directed acyclic graph  $\mathcal{G}$  whose nodes represent variables  $Z_1, \dots, Z_p$  and whose edges represent causal relationships. Specifically, each variable  $Z_k$  is defined via the equation  $Z_k = f_k(Z_{\text{PA}_G(k)}, \varepsilon_k)$ , where  $f_k$  is a deterministic function,  $\text{PA}_G(k)$  denotes the parents of  $Z_k$ , and  $\varepsilon_1, \dots, \varepsilon_p$  are independent “exogenous” random variables. SCMs have long been used to model causal inference from observational data, in which case  $f_1, \dots, f_p$  are usually defined to be linear functions. Instead, TabPFN allows them to be neural networks or decision trees, thereby modeling nonlinear and even discontinuous structure.

These two key ideas cohere to provide an efficient training strategy for TabPFN. To fit the model’s parameters  $\theta$ , a collection  $\mathfrak{D}$  of approximately 130M synthetic datasets were generated. Each dataset  $\mathcal{D} \in \mathfrak{D}$  contains IID examples from a joint distribution  $\pi$ , which is itself drawn uniformly from the SCM prior. Note that while  $\pi$  may have a complex density, the SCM structure gives a simple way to sample from it.

Next,  $\mathcal{D}$  is partitioned into a “pseudo”-training set  $\mathcal{D}_{\text{train}}$  and “pseudo”-test set  $\mathcal{D}_{\text{test}}$ . For each  $(X_{\text{test}}, Y_{\text{test}}) \in \mathcal{D}_{\text{test}}$ , the transformer output  $M_\theta(X_{\text{test}}, \mathcal{D}_{\text{train}})$  approximates the PPD  $p(\cdot | X_{\text{test}}, \mathcal{D}_{\text{train}})$ . The loss

$$\frac{1}{|\mathfrak{D}|} \sum_{\substack{\mathcal{D} \in \mathfrak{D} \\ (X_{\text{test}}, Y_{\text{test}}) \in \mathcal{D}_{\text{test}}}} \log M_\theta(X_{\text{test}}, \mathcal{D}_{\text{train}})(Y_{\text{test}})$$

can be showed to be an unbiased estimate of the conditional KL divergence between the true and approximate PPDs, and is minimized via stochastic gradient descent. We refer the reader to Hollmann et al. [30] for further details on the prior as well as on model training.

Both the NP and PFN approaches use a “meta-learning” perspective to approximate the PPD, but they differ in their implementation choices. NPs employ an encoder-decoder architecture with a parametric distribution over the latent variable  $z$ , naturally lending itself to variational inference. PFNs, on the other hand, adopt a transformer architecture that avoids explicit distributional assumptions in its internal representations. As a result, their training objectives differ slightly: NPs explicitly optimize a variational lower bound, while PFNs frame learning as a direct optimization problem.

### 3. CASE STUDIES

#### 3.1 Study I: parameter estimation in a semi-supervised setting

**3.1.1 Problem and motivation** In regression and classification problems, labeled data are often scarce or costly to obtain, while unlabeled data are typically more abundant. This abundance arises because unlabeled data (e.g., medical images, sensor readings, or customer transactions) are often generated organically during routine operations, whereas the corresponding labels (e.g., diagnoses, system states, or purchase intentions) require expert annotation or time-consuming measurement. Semi-supervised learning methods (SSL) [58] attempt to improve the efficiency of statistical analyses on the labeled data by leveraging information contained in unlabeled data, usually under the assumption that both sets of data share the same data-generating distribution.

We consider the problem of parameter estimation in an SSL setting. To formalize this, let  $X \in \mathbb{R}^p$  denote the feature vector and  $Y \in \mathbb{R}$  the response variable. We observe:

- A labeled dataset  $\mathcal{D}_L = \{(X_i, Y_i)\}_{i=1}^n$  with  $n$  IID observations from the joint  $P_{X,Y}$ ;
- An unlabeled dataset  $\mathcal{D}_U = \{X_i\}_{i=n+1}^{n+m}$  with  $m$  IID observations from the marginal  $P_X$ .

The goal is to estimate a parameter  $\theta$  of  $P_{X,Y}$ , such as the mean of  $P_Y$  or the regression coefficients of  $Y$  on  $X$ . Generalizing earlier work, Song, Lin and Zhou [49] and Angelopoulos et al. [1] both considered an M-estimation framework, in which the parameter  $\theta \in \mathbb{R}^q$  is defined as the minimizer of the expected loss:

$$(1) \quad \theta^* := \arg \min_{\theta \in \Theta} \mathbb{E}_{P_{X,Y}} \{l(\theta; X, Y)\},$$

where  $l : \Theta \times \mathbb{R}^p \times \mathbb{R} \rightarrow \mathbb{R}$  is a pre-specified loss function. Examples of such estimands are shown in Table 1. Note that these working models do not have to be correctly specified in order for the estimands to be meaningful.

TABLE 1  
Parameters of interest in the three simulation settings. Here we define  $\vec{X} = [1, X^\top]^\top$  and  $\tau \in (0, 1)$  is a given value.

Setting	Parameter of Interest: $\theta$
1 (linear reg.)	$\left\{ \mathbb{E}(\vec{X} \vec{X}^\top) \right\}^{-1} \mathbb{E}(\vec{X} Y)$
2 (logistic reg.)	$\arg \min_{\theta} \mathbb{E} \left\{ \log \left[ 1 + \exp(\vec{X}^\top \theta) \right] - Y \vec{X}^\top \theta \right\}$
3 (quantile reg.)	$\arg \min_{\theta} \mathbb{E} \left\{ \left[ I(Y \leq \vec{X}^\top \theta) - \tau \right] (Y - \vec{X}^\top \theta) \right\}$

**3.1.2 State-of-the-art** We describe two recently proposed methodologies. To do so, we first define the empirical risk minimizer with respect to a labeled dataset  $\mathcal{D}$  as:

$$(2) \quad \hat{\theta}_{\text{ERM}}(\mathcal{D}) = \arg \min_{\theta \in \Theta} \sum_{(X, Y) \in \mathcal{D}} l(\theta; X, Y).$$

- Angelopoulos et al. [1] proposed a simple imputation and debiasing framework that makes use of an existing black-box regression or classification model  $M$ : (a) Use  $M$  to impute labels  $\hat{Y}_i$  on both the labeled and unlabeled datasets. Denote these imputed datasets as  $\hat{\mathcal{D}}_L = \{(X_i, \hat{Y}_i)\}_{i=1}^n$  and  $\hat{\mathcal{D}}_U = \{(X_i, \hat{Y}_i)\}_{i=n+1}^{n+m}$  respectively; (b) Estimate the imputation bias via:  $\Delta = \hat{\theta}_{\text{ERM}}(\hat{\mathcal{D}}_L) - \hat{\theta}_{\text{ERM}}(\mathcal{D}_L)$ ; (c) Return the estimate  $\hat{\theta}_{\text{ERM}}(\hat{\mathcal{D}}_U) - \Delta$ .
- Song, Lin and Zhou [49] (**SLZ**) proposed a method that makes a projection-based correction to the ERM loss (2). They proved that their method has optimal asymptotic efficiency under certain assumptions and further showed superior performance over other methods [4, 12, 31] via numerical experiments. On the other hand, their method requires hyperparameter tuning such as a choice of the projection space.

**3.1.3 Experimental design** We repeat Song, Lin and Zhou [49]’s experiments, but add two comparators that make use of TabPFN:

- TabPFN-Debiased (TabPFN-D):** Following Angelopoulos et al. [1]’s approach, we impute each label using the posterior predictive mean (for continuous labels) or mode (for discrete labels), with PPD approximated by TabPFN supplied with  $\mathcal{D}_L$  as a training set.<sup>3</sup> However, return the estimate  $\hat{\theta}_{\text{ERM}}(\hat{\mathcal{D}}_L \cup \hat{\mathcal{D}}_U) - \Delta$  (i.e. solve ERM on the union of imputed versions of both the labeled and unlabeled datasets).
- TabPFN-Imputed (TabPFN-I):** Follow the same approach as in TabPFN-D, but return the ERM solution without debiasing:  $\hat{\theta}_{\text{ERM}}(\hat{\mathcal{D}}_L \cup \hat{\mathcal{D}}_U)$ .

We use the original authors’ implementation for the SLZ method. As a further baseline, we consider the estimator  $\hat{\theta}_{\text{ERM}}(\mathcal{D}_L)$  that only makes use of labeled data (**Vanilla**).

We consider three types of estimands, corresponding to parameters from linear, logistic, and quantile regression working models (Table 1). These are called “working models” because the true data-generating process differs from the estimation models. We vary:

- Feature dimensions:  $p \in \{4, \dots, 9\}$
- Sample sizes:  $n \in \{300, 500\}$  (labeled),  $m \in \{500, 1000, 2000\}$  (unlabeled)
- Quantile levels (Setting 3 only):  $\tau \in \{0.25, 0.5\}$

yielding at least  $6 \times 2 \times 3 = 36$  configurations. For each configuration, we approximate the true  $\theta^*$  via Monte Carlo integration using  $10^7$  samples. Using 500 replicates for each configuration, we compute estimates for  $\theta^*$ , and use them to estimate the bias and mean squared error (MSE). Further experimental details are given in Appendix A.

**3.1.4 Results** Representative results of our experiments are shown in Figure 1, with the complete set of results deferred to Appendix A. The first three panels (from the left) show MSE with respect to linear, logistic, and quantile regression respectively when  $p = 5$ , with various combinations of  $(n, m)$ . In the last panel, we show how the results for logistic regression vary with  $p$ , observing that SLZ is only able to outperform the TabPFN approaches when  $p = 4$ . In general, we observe that TabPFN-I and TabPFN-D significantly outperform SLZ in terms of MSE. We also decompose MSE into squared bias (shaded bar) and variance (solid bar) for the four methods and observe that while TabPFN-I has larger bias than TabPFN-D (as well as other two methods), it has significantly smaller variance, which offsets larger bias and leads to smaller MSE.

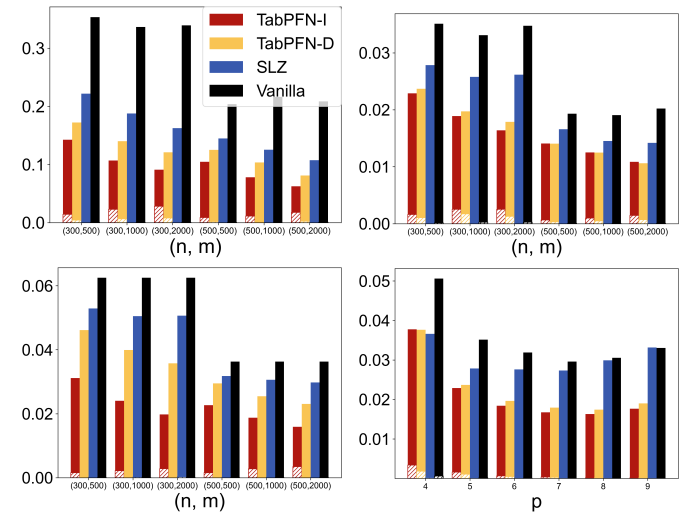


Fig 1: MSE results for linear (top left), logistic (top right), and quantile ( $\tau = 0.25$ , bottom left) regressions when  $p = 5$ . MSE results for the logistic regression with various  $p$  (bottom right) when  $(n, m) = (300, 500)$ .

<sup>3</sup>Angelopoulos et al. [1] do not specify how to fit the imputation model.

**3.1.5 Real data comparison** To evaluate performance in real-world scenarios, we test the methods on ten OpenML datasets [20], comprising five for regression and five for binary classification. For each dataset, we first establish a ground truth target parameter by fitting a linear model (for regression) or a logistic regression model (for classification) on the full dataset. We then create labeled-unlabeled splits by randomly selecting  $n$  observations as labeled data—with  $n$  set to 10% of the full dataset for regression and 20% for classification<sup>4</sup>—and treating the remainder as unlabeled (using only their features). From these splits, we compute the Vanilla, TabPFN-I, TabPFN-D, and SLZ estimators. In the logistic regression setting, we alternately explore using imputation using the posterior predictive mean for TabPFN-I and TabPFN-D, a procedure that has also been called fractional imputation [47].<sup>5</sup> We repeat this process 50 times and report the average MSE of the estimated coefficients across all repetitions. The data-selection criteria and dataset details are provided in Appendix A.3.

TABLE 2  
Real data SSL: Linear regression. Values represent  $\times 10^{-4}$  of the metric

ID	Vanilla	TabPFN-I	TabPFN-D	SLZ
189	6.3621	2.3105	1.8860	6.5636
218	15.2800	4.3926	2.5916	$3.1214 \times 10^{10}$
225	7.0790	1.5684	3.0303	7.0924
1200	1.9185	0.8884	0.7787	1.7529
45052	74.5046	100.3051	64.2511	80.6998

TABLE 3  
Real data SSL: Logistic regression

ID	Vanilla	TabPFN-I	TabPFN-D	TabPFN-I	TabPFN-D	SLZ
				mode imputation	mean imputation	
251	0.0195	2.6087	0.2679	0.0149	0.0181	0.0200
807	0.0036	0.0116	0.0065	0.0020	0.0017	0.0037
816	0.0060	0.1081	0.01550	0.0026	0.0044	0.0060
1046	0.0025	0.0030	0.0022	0.0013	0.0011	0.0025
40983	5.5566	2.3351	2.5356	1.2346	1.9884	5.9513

The results for linear and logistic regression are presented in Table 2 and Table 3, respectively. For linear regression, both TabPFN-I and TabPFN-D typically

<sup>4</sup>For numerical stability, we further constrained  $n$  to be at least 5,000.

<sup>5</sup>Fractional imputation replaces each observation with a missing binary response by the two pseudo-observations with responses 1 and 0 and sample weights  $P(Y = 1 | X = x)$  and  $P(Y = 0 | X = x)$ . This yields the same contribution to the score function as imputing the missing response with the single mean value  $\sum_{y \in \{0,1\}} y P(Y = y | X = x) = P(Y = 1 | X = x)$ .

outperform the Vanilla and SLZ methods. TabPFN-D’s slight advantage over TabPFN-I suggests a benefit from debiasing in these presumably more noisy and complicated settings. For logistic regression, Vanilla outperforms SLZ and TabPFN with mode imputation, whereas TabPFN with mean imputation achieves the best performance. We attribute the weaker performance of mode imputation to its inherent bias: it deterministically assigns a class label even when predictions are uncertain, whereas mean imputation preserves uncertainty by weighting labels according to predicted probabilities, improving stability and accuracy [47].

### 3.2 Study II: heterogeneous treatment effects estimation

**3.2.1 Problem and motivation** While researchers were previously satisfied with estimating the average effect of a treatment—such as a drug, social intervention, or economic policy—across a population of interest, there has been rising interest in estimating heterogeneous treatment effects (HTE), that is, how different groups of individuals might benefit differentially from the same treatment. Accurate HTE estimation enables personalized treatments, which may lead to better outcomes.

HTE is usually quantified via the Neyman–Rubin potential outcomes framework [46]. We consider  $n$  IID samples  $(Y_i(0), Y_i(1), T_i, X_i)$  from a population, where  $X_i \in \mathbb{R}^d$  is a  $d$ -dimensional feature vector,  $T_i \in \{0, 1\}$  is a binary treatment assignment indicator, and  $Y_i(0)$  and  $Y_i(1) \in \mathbb{R}$  are potential outcomes. The observed outcome is  $Y_i^{\text{obs}} = Y_i(T_i)$ . Define the response functions under control and treatment respectively as

$$\mu_j(x) = \mathbb{E}[Y(j) | X = x], \quad j = 0, 1,$$

and the conditional average treatment effect (CATE) function as  $\tau(x) = \mu_1(x) - \mu_0(x)$ . The propensity score is defined as  $e(x) = \mathbb{E}(T | X = x)$ . Unlike the average treatment effect (ATE)  $\tau = \mathbb{E}[\tau(X)]$ , the CATE captures HTE and is hence our estimand of interest.

**3.2.2 State-of-the-art** Many methods have recently been proposed to estimate the CATE under the assumption of ignorability  $((Y(1), Y(0)) \perp\!\!\!\perp T | X)$ . Most but not all of these methods can be subsumed under Künzel et al. [34]’s framework for “meta-learners”, which they defined as “the result of combining supervised learning or regression estimators (i.e., base learners) in a specific manner while allowing the base learners to take any form”. These include:

- **S-Learner:** (a) Form an estimate  $\hat{\mu}(t, x)$  for the function  $(t, x) \mapsto \mu_t(x)$  by jointly regressing  $Y_i^{\text{obs}}$  on  $T_i$  and  $X_i$ ; (b) Set  $\hat{\tau}_S(x) = \hat{\mu}(1, x) - \hat{\mu}(0, x)$ .

- **T-Learner**: (a) Form estimates  $\hat{\mu}_0(x), \hat{\mu}_1(x)$  for  $\mu_0(x)$  and  $\mu_1(x)$  by regressing  $Y_i^{\text{obs}}$  on  $X_i$  within the control and treatment groups respectively; (b) Set  $\hat{\tau}_T(x) = \hat{\mu}_1(x) - \hat{\mu}_0(x)$ .
- **R-Learner** [39]: (a) Form estimates  $\hat{e}(x)$  for  $e(x)$  and  $\hat{m}(x)$  for  $m(x) = \mathbb{E}(Y_i^{\text{obs}} | X_i = x)$ ; (b) Compute residuals  $\tilde{Y}_i = Y_i^{\text{obs}} - \hat{m}(X_i)$ ,  $\tilde{T}_i = T_i - \hat{e}(X_i)$ ; (c) Solve

$$(3) \quad \hat{\tau}_R(\cdot) = \arg \min_{\tau} \frac{1}{n} \sum_{i=1}^n (\tilde{Y}_i - \tau(X_i) \tilde{T}_i)^2.$$

- **DR-Learner** [32]: (a) Form estimates  $\hat{\mu}_0(x)$  for  $\mu_0(x)$ ,  $\hat{\mu}_1(x)$  for  $\mu_1(x)$ , and  $\hat{e}(x)$  for  $e(x)$ ; (b) Compute doubly robust pseudo-outcomes  $\tilde{Y}_i$  using these models<sup>6</sup>; (c) Form an estimate  $\hat{\tau}_{\text{DR}}(x)$  for  $\tau(x)$  by regressing  $\tilde{Y}_i$  on  $X_i$ .
- **X-Learner** [34]: (a) Form estimates  $\hat{\mu}_0(x)$  for  $\mu_0(x)$  and  $\hat{\mu}_1(x)$  for  $\mu_1(x)$ ; (b) Impute treatment effects:  $\tilde{D}_i^1 = Y_i^{\text{obs}} - \hat{\mu}_0(X_i)$  (treatment group) and  $\tilde{D}_i^0 = \hat{\mu}_1(X_i) - Y_i^{\text{obs}}$  (control group); (c) Form preliminary estimates  $\hat{\tau}_j(x)$  for  $\tau(x)$  by regressing  $\tilde{D}_i^0$  on  $X_i$  for  $j = 0, 1$ ; (d) Combine the two estimates via  $\hat{\tau}_X(x) = g(x)\hat{\tau}_0(x) + (1 - g(x))\hat{\tau}_1(x)$  (typically  $g(x) = \hat{e}(x)$ ).

Foster and Syrgkanis [21] advocated for either the R-Learner or DR-Learner as, unlike the S-, T- and X-Learners, they satisfy Neyman orthogonality, which result in theoretically faster estimation rates so long as the base learners used to estimate the nuisance parameters (e.g.  $e(x)$  and  $m(x)$ ) satisfy certain convergence properties. They used Wang et al. [55]’s AutoML algorithm<sup>7</sup> as the base learner in the meta-leaner strategies detailed above, and showed that the R-Learner or DR-Learner indeed achieved better performance.

**3.2.3 Experimental design** We repeat Foster and Syrgkanis [21]’s experiments, but add TabPFN as a choice of base learner. We compare the five meta-learner strategies detailed above, together with an “oracle” comprising the R-Learner fitted with the true nuisance functions  $m(x)$  and  $e(x)$ . Note that the optimization problem (3) for the R-Learner is solved via weighted least squares. Since TabPFN currently does not support weighted loss minimization, this means that it cannot be used as a base learner for both the R-Learner and oracle methods. This results in 10 total estimators (2 base learners  $\times$  6 methods – 2 exclusions). Each estimator is named by its method followed

$$6\tilde{Y}_i = \frac{T_i(Y_i - \hat{\mu}_1(X_i))}{\hat{e}(X_i)} - \frac{(1 - T_i)(Y_i - \hat{\mu}_0(X_i))}{1 - \hat{e}(X_i)} + \hat{\mu}_1(X_i) - \hat{\mu}_0(X_i)$$

<sup>7</sup>AutoML uses cross-validation (CV) and a smart exploration strategy to select from a collection of the most popular machine learning models and to tune their hyperparameters.

by the base learner in parentheses (e.g., ‘S-Learner (TabPFN)’).

In each experiment, we generate a dataset according to the Neyman-Rubin model detailed above, with  $X_i \sim \text{Unif}([-0.5, 0.5]^6)$  and  $Y_i(t) = \mu_t(X_i) + \epsilon_i$  for  $t = 0, 1$ , where  $\epsilon_i \sim \mathcal{N}(0, \sigma^2)$ . We explore 6 different configurations of the functions  $e(x)$ ,  $\tau(x)$  and  $b(x) = (\mu_0(x) + \mu_1(x))/2$ , but due to space limits, present only the two representative cases in the main paper:

- **Setup A**: complicated  $e(x)$  and  $b(x)$ , but a relatively simple  $\tau(x)$ .
- **Setup E**: large  $b(x)$  resulting in substantial confounding, discontinuous  $\tau(x)$ .

Complete specifications of the functional forms and other settings are given in Appendix B. We vary two key experimental parameters: the training set size  $n$  and noise level  $\sigma^2$ . For evaluation, we generate a fixed test set of size 10000 and report the MSE of the estimated treatment effect function evaluated on the test set.

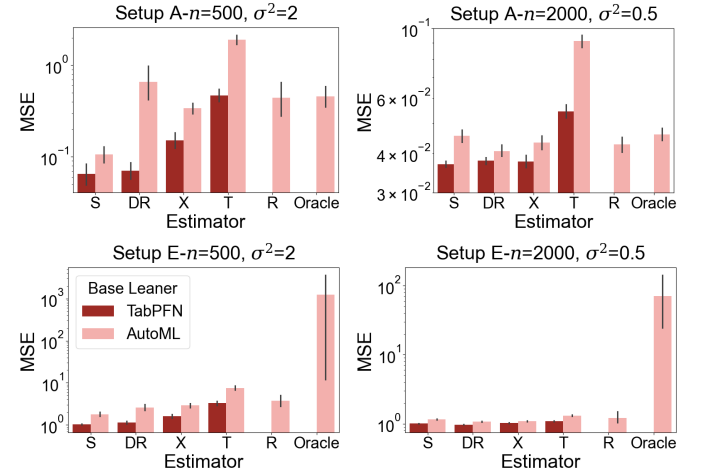


Fig 2: Test MSE of various CATE estimators under Setup A (top) and Setup E (bottom) over 100 repetitions. The left panels show results for the small-sample, high-variance scenario ( $n = 500, \sigma^2 = 2$ ), while the right panels display the large-sample, low-variance scenario ( $n = 2000, \sigma^2 = 0.5$ ).

**3.2.4 Results** We display the results for Setup A and E in Figure 2 and defer the complete set of experimental results to Table 7 in Appendix B. Most strikingly, across all experimental settings, using TabPFN as the base learner in a meta-learner strategy greatly improves upon its AutoML counterpart. Second, despite its lack of Neyman orthogonality or double robustness, S-Learner (TabPFN) achieves the best accuracy in most settings and is among the top two

performers in almost all settings. Our results stand in contrast to those of Foster and Syrgkanis [21] and most of the current HTE literature, which has tended to de-emphasize the role played by the base learner because the error it accrues when estimating the nuisance parameters becomes second-order for the R- and DR-Learners under what they consider to be relatively mild conditions. The superior performance of S-Learner (TabPFN) shows that this asymptotic regime is sometimes not attained even under relatively simple simulation settings, and that the choice of base learner can be as important as the choice of metalearner framework. Indeed, the superior regularization of TabPFN compared to other regression estimators may have a special synergy with the S-Learner strategy, resulting in its superior accuracy, especially in low sample size and signal-to-noise ratio (SNR) settings.

**3.2.5 Real data comparison** We evaluate the TabPFN-based meta-learners on the semi-synthetic ACIC 2017 competition benchmark based on the IHDP covariates [8, 17, 26]. The benchmark provides 6,000 datasets generated from real covariates under a controlled set of data-generating processes (DGPs), varying (i) the error structure (IID, non-additive, and group-correlated), (ii) the selection strength  $\kappa$  (i.e. variability of the true propensity score), (iii) the treatment effect size, and (iv) the noise level. Each scenario includes ground-truth CATEs, allowing performance assessment by RMSE. We compare the four TabPFN-based meta-learners (S-, T-, X-, and DR-Learner) against the 16 methods described in Hahn, Dorie and Murray [26] that are reported with complete benchmark results. These methods notably include Causal Forests (GRF, Athey, Tibshirani and Wager [3]), Targeted Learning (TL, Coyle et al. 14), various versions of BART, and Bayesian Causal Forests (BCF, Hahn, Murray and Carvalho 27), all of which are considered in the literature to be strong baselines. We do not compare with the AutoML-based metal-learners due to the much higher computational overhead required in comparison with using TabPFN.

Figure 3 reports the RMSE of each method averaged within each error type and selection strength level. Under weak selection strength, all TabPFN-based estimators match or outperform the baselines. Under strong selection strength, their performance degrades somewhat, which we believe is due to the phenomenon of regularization-induced confounding described in Hahn, Murray and Carvalho [27]—an issue that BCF was specifically designed to fix. Borrowing an idea from BCF, we enhanced the S-, T-, X-Learners by first fitting a propensity score model using

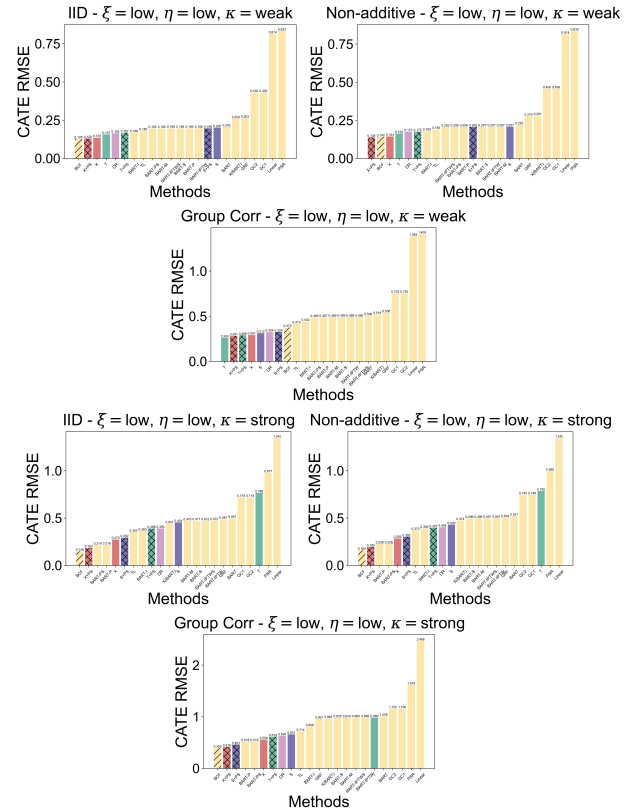


Fig 3: RMSE of TabPFN-based CATE estimators against SOTA methods on the ACIC 2017 benchmark. Results are shown across panels organized by error type (columns) and selection strength  $\kappa$  (rows). Colored bars represent meta-learners built on TabPFN: S-Learner, T-Learner, X-Learner, DR-Learner. The S-, T-, and X-learners enhanced with a propensity score covariate are indicated with the same colors but decorated with a shaded pattern. Bayesian Causal Forests is shown as the shaded yellow bar.

a TabPFN classifier and then use the fitted score values as an additional covariate when fitting each base learner model.<sup>8</sup> Under strong selection strength, the resulting methods, especially the X-Learner, all enjoy improved performance that is competitive with the state-of-the-art. Finally, we note that the DR-learner, despite its semi-parametric optimality guarantees, again does not have the best performance in any setting. Full experimental details and per-scenario results are provided in Appendix B.2.

### 3.3 Study III: prediction under covariate shift

**3.3.1 Problem and motivation** In regression and classification problems, covariate shift refers to the scenario where the marginal covariate distribution  $p(x)$

<sup>8</sup>The variant is not used for the DR-learner since it already makes use of the propensity score to impute pseudo-outcomes.

differs between training and test datasets, while the predictive distribution  $p(y|x)$  remains the same. This distributional mismatch frequently arises in real-world applications—for instance, due to outdated training data or sampling biases between datasets. Since covariate shift can substantially degrade model performance, it has become an active area of research [42, 43, 56].

More precisely, we observe a training dataset  $\mathcal{D}_s$  comprising  $n$  IID observations from a source distribution  $p_s(x)p(y|x)$  and wish to predict the responses on a test dataset  $\mathcal{D}_t$  comprising  $m$  IID observations from the target distribution  $p_t(x)p(y|x)$ , with accuracy evaluated via prediction MSE. Furthermore,  $p_s(x)$  and  $p_t(x)$  are usually unknown.

**3.3.2 State-of-the-art** Classical approaches to address covariate shift make use of importance weighting techniques. More recently, the problem has been studied under the assumption that the regression function  $f(x) = \mathbb{E}(Y|X=x)$  has bounded norm in a reproducing kernel Hilbert space, in which case kernel ridge regression (KRR) with a carefully tuned regularization parameter  $\lambda$  was shown to achieve optimal rates, whereas a naïve, unadjusted estimator is suboptimal [36]. Wang [54] introduced a method based on “pseudo-labeling” (**PL**) for selecting  $\lambda$ , claiming that it improves upon Ma, Pathak and Wainwright [36]’s work by relaxing certain distributional assumptions. Specifically, PL fits KRR on the first half of  $\mathcal{D}_s$  and uses the fitted model to impute labels for an auxiliary unlabeled dataset  $\tilde{\mathcal{D}}_t$  drawn from  $p_t(x)$ . It then fits a collection of KRR models with different  $\lambda$  parameters on the second half of  $\mathcal{D}_s$  and uses  $\tilde{\mathcal{D}}_t$  with the imputed labels to select the best-performing model.

**3.3.3 Experimental design** We repeat Wang [54]’s experiments, but add a simple comparator approach which directly fits a model on  $\mathcal{D}_s$  using **TabPFN** and does not make any adjustment. In addition to PL, the following methods were used as comparators:

- **Naive**: Fit a gradient boosting regression model on  $\mathcal{D}_s$ , tuned using five-fold CV.
- **Importance-Weighted (IW)**: Fit a gradient boosting model on  $\mathcal{D}_s$  similarly to the naive approach, but with the loss function weighted by the true density ratio  $p_t(x)/p_s(x)$ .
- **Wang-Oracle**: A variant of PL where the true conditional mean  $\mathbb{E}(Y|X=x)$  is used for  $\tilde{\mathcal{D}}_t$  instead of imputed values. This serves as an oracle benchmark within Wang [54].

We consider univariate covariate distributions that are Gaussian mixtures. The training and test distributions have the same components but differ in their mixing

weights:

$$p_s = \frac{5}{6}\text{Unif}(0, 0.5) + \frac{1}{6}\text{Unif}(0.5, 1),$$

$$p_t = \frac{1}{6}\text{Unif}(0, 0.5) + \frac{5}{6}\text{Unif}(0.5, 1).$$

The response variable follows  $Y|X=x \sim \mathcal{N}(f(x), 1)$ , where we investigate five distinct mean functions: (i)  $f(x) = \cos(2\pi x) - 1$ ; (ii)  $f(x) = \sin(2\pi x)$ ; (iii)  $f(x) = |x - 1/2| - 1/2$ ; (iv)  $f(x) = f_1(x) + f_2(x) - 2$ ,  $f_1(x) = \min\{1, \max\{4x - 1, 0\}\}$  and  $f_2(x) = \min\{1, \max\{4x - 3, 0\}\}$ ; (v)  $f(x) = x \sin(4\pi x)$ . In each experiment, we generate training and test datasets as described above, with the size of the test set fixed at  $m = 10^4$ , while we vary the training set size  $n \in \{500, 600, \dots, 1200\}$ . The results are averaged over 500 replicates.

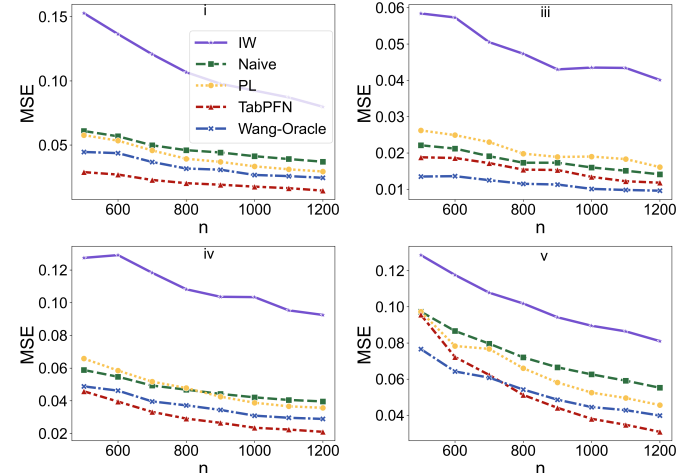


Fig 4: Comparison of prediction MSE for different covariate shift methods across varying sample sizes ( $n$ ) and scenarios.

**3.3.4 Results** Figure 4 shows the prediction MSE as a function of  $n$  for all five methods, with respect to the mean functions (i), (iii), (iv), and (v) (results for setting (ii), which shows similar patterns to (i), are provided in Appendix C). We observe that TabPFN consistently outperforms the PL method, even matching or exceeding the oracle method’s performance at larger sample sizes ( $n \geq 800$ ), in all settings apart from (iii). This is despite TabPFN not making use of the auxiliary information in  $\tilde{\mathcal{D}}_t$  required by PL and the oracle method.

**3.3.5 Real data comparison** To assess performance beyond the univariate synthetic setting of Wang [54], we evaluate the methods on two multivariate UCI regression datasets: *Airfoil Self-Noise* ( $n = 1503$ , 5 covariates) and *Concrete Compressive Strength* ( $n =$

1030, 8 covariates). For each dataset, we perform a 70/30 train–test split and resample the test set with replacement using weights  $\omega(x) = \exp(x^\top \beta)$  following the procedure introduced by Tibshirani et al. [51]. Two shift vectors  $\beta$  are considered per dataset, and results are averaged over 10 repetitions. Table 4 reports the mean prediction MSE and standard error across repetitions. Across all datasets and shift settings, TabPFN achieves the best predictive accuracy, often by a substantial margin. Full experimental details are provided in Appendix C.2.

TABLE 4  
Average PMSE (mean  $\pm$  standard error) over 10 random splits under covariate shift. Each dataset is evaluated under two  $\beta$  settings.

Dataset	Setting	Wang-Oracle	PL	Naïve	IW	TabPFN
Airfoil	$\beta_1$	$13.07 \pm 2.09$	$14.49 \pm 2.15$	$10.25 \pm 3.33$	$21.46 \pm 7.07$	$3.20 \pm 0.84$
	$\beta_2$	$8.29 \pm 0.72$	$8.85 \pm 0.81$	$3.73 \pm 0.57$	$3.46 \pm 0.90$	$1.71 \pm 0.22$
Concrete	$\beta_1$	$48.72 \pm 15.83$	$109.15 \pm 24.72$	$5.50 \pm 1.30$	$5.36 \pm 1.85$	$2.27 \pm 0.45$
	$\beta_2$	$63.10 \pm 19.42$	$116.68 \pm 26.49$	$7.72 \pm 0.84$	$7.78 \pm 2.02$	$4.89 \pm 0.70$

## 4. TABPFN ADAPTIVITY

In this section, we illustrate the adaptivity of TabPFN, which we believe provides a compelling explanation for its strong predictive performance across a wide range of tasks, as demonstrated in the previous sections. By adaptivity, we refer to the ability of a procedure to automatically adjust to unknown properties of the underlying data-generating process while still achieving near-optimal performance. This notion has deep roots in nonparametric statistics, where it was classically studied in the context of regression. Foundational work by Lepskii [35], and later by Donoho and Johnstone [16], established estimators that could adapt to unknown smoothness levels of a target function, achieving optimal rates without prior specification of regularity.

However, the form of adaptivity exhibited by TabPFN appears both different and broader. Unlike traditional methods that adapt within a single nonparametric framework—typically modulating local smoothness or bandwidth—TabPFN seems capable of flexibly behaving like a highly nonparametric method when the signal is irregular, yet also exploiting parametric structure when present. In other words, rather than committing to either a parametric or nonparametric regime, TabPFN dynamically adjusts across these regimes, a property that is rare among classical estimators. We will investigate this property in the context of both regression and classification.

### 4.1 Adaptivity in regression

To investigate adaptivity in regression, we consider the problem of sparse linear regression and compare the performance of TabPFN against that of specialized methods, namely LASSO, SCAD, and MCP regression, across a range of data-generating settings. We find that TabPFN can outperform these methods and can even be used to estimate regression parameters with smaller bias than LASSO. To complement this analysis, we also perform a visual comparison of TabPFN with Gaussian process regression in Section D, observing that the two methods perform similarly, but with subtle differences in their inductive biases.

4.1.1 *Experimental design* We follow the experimental design of Hastie, Tibshirani and Tibshirani [28] and generate  $Y = X^\top \beta^* + \epsilon$ , with two types of  $\beta^* \in \mathbb{R}^p$  having sparsity  $s$  (*i.e.*,  $s$  entries are 1 and the rest are 0):

- Beta-type I:  $\beta^*$  has  $s$  components equal to 1, spaced approximately evenly across the  $p$  indices, and the rest equal to 0;
- Beta-type II:  $\beta^*$  has its first  $s$  components equal to 1, and the rest equal to 0.

Features corresponding to non-zero (zero) coefficients are termed relevant (irrelevant). We fix  $p = 100$  and vary  $s \in \{1, 5, 10, 20, 30\}$ . The features  $\{x_i : i \in [n]\}$  are drawn i.i.d. from  $\mathcal{N}_p(0, \Sigma)$ , where  $\mathcal{N}_p$  denotes a  $p$ -dimensional Gaussian and  $\Sigma$  is either the identity matrix or a matrix with  $(i, j)$ -th entry equal to  $0.35^{|i-j|}$  (banded correlation). Since beta-type I and II are equivalent when  $\Sigma$  is identity, this gives 3 distinct experimental scenarios. The response  $y_i$  is generated with additive Gaussian noise, whose variance  $\sigma^2$  is chosen to meet the desired signal to noise ratio (SNR), denoted by  $\nu$ . Specifically, we set  $\sigma^2 = (\beta^*)^\top \Sigma \beta^* / \nu$ . We consider SNR values  $\nu \in \{0.05, 0.25, 1.22, 6\}$ , spanning low to high noise regimes. Finally, we select  $n \in \{50, 500\}$ . This yields  $5$  (sparsity)  $\times$   $3$  (beta and design matrix)  $\times$   $4$  (SNR)  $\times$   $2$  (sample size) = 120 experimental settings. For each setting, we evaluate performance on an independent test set of size 1000, with the results averaged over 100 experimental replicates. Regularization parameters for comparators is tuned using 5-fold cross-validation.

4.1.2 *Prediction performance comparison* In Figure 5, we plot the relative test MSE (averaged over 100 repetitions) of the comparator methods to that of TabPFN. We focus on the orthogonal feature case, with the results for correlated features deferred to Appendix E.2. Compared to LASSO, we observe that TabPFN tends to perform better for  $s \leq 10$ , with

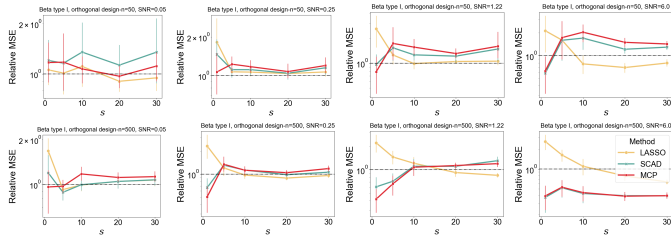


Fig 5: Relative test MSE compared to TabPFN, using a beta-type I orthogonal design. Rows show results for  $n = 50$  (top) and  $n = 500$  (bottom); columns show increasing SNR.

the performance gap increasing for higher sample size and SNR. Conversely, compared to SCAD and MCP, TabPFN tends to perform better for  $s \geq 5$  and for lower sample size and SNR. In other words, TabPFN seems to achieve a type of middle-ground between the two classes of methods.

**4.1.3 Descriptive accuracy** Beyond predictive accuracy, we also consider the descriptive accuracy of the TabPFN model—how well does it reflect the sparse linear generating model and how it may be used to estimate the true regression coefficients. We can visually inspect the fitted TabPFN model using Accumulated Local Effects (ALE) plots, which summarize the dependence of the model on each individual feature [2].<sup>9</sup> Figure 21 in the Appendix exhibits the results when the features are orthogonal. We observe that for moderate to high SNR ( $\geq 1.22$ ), almost all ALE plots of relevant features are roughly linear. In addition, when  $n = 500$ , the ALE plots for the irrelevant features display much less variation, which suggests that the TabPFN model is indeed well-approximated by a low-dimensional linear surface. For smaller SNR, the ALE plots are generally nonlinear and are not shown.

The linearity of the ALE plots suggests a two-step pipeline for using TabPFN to estimate the true regression coefficients: We first fit a TabPFN model to the data and then fit an ordinary least squares model to the TabPFN fitted values. In Table 5, we compare the accuracy of this procedure to that of LASSO, SCAD, and MCP, further breaking down the error into squared bias and variance. For smaller values of  $s$ , we observe that the TabPFN performs similarly to SCAD and MCP: Its coefficients have much smaller bias compared to LASSO while having comparable variance, thus avoiding the well-known tendency of LASSO to bias its estimates via shrinkage.

<sup>9</sup>ALE plots avoid both the confounding associated with conditional dependence plots and the out-of-sample instability associated with marginal dependence plots.

## 4.2 Adaptivity in classification

We examine the classification performance of TabPFN in the presence of label noise, that is, when the observed labels  $\tilde{Y}_1, \tilde{Y}_2, \dots, \tilde{Y}_n$  in our training set are corrupted from their true values  $Y_1, Y_2, \dots, Y_n$ , such as by coding errors. For simplicity, we consider homogeneous noise in a binary class setting:  $\mathbb{P}(\tilde{Y} \neq Y|X = x, Y = y) = \rho, y \in \{0, 1\}$ , where  $\rho$  is the corruption fraction. The goal is to train a classifier to predict the *original* label, namely, we want to estimate a mapping  $C: \mathbb{R}^d \rightarrow \{0, 1\}$  minimizing the risk  $R(C) = \mathbb{E}[C(X) \neq Y]$ .

This problem is especially interesting when the conditional distribution of the true label,  $p(Y|X = x)$ , has a simple parametric form. For example, if  $X|Y = y$  is Gaussian, the noise-free classification problem can be solved efficiently via linear discriminant analysis (LDA). On the other hand, the conditional distribution of the corrupted label,  $p(\tilde{Y}|X = x)$ , does not have the correct functional form, which makes LDA inconsistent. In comparison, Cannings, Fan and Samworth [10] proved that  $k$ -nearest neighbors ( $k$ NN) and kernelized support vector machines (SVM) can be robust to label noise. However, these methods, which are based on local averaging, pay a price in terms of being less efficient when the labels are noise free.

We show that TabPFN is able to break this robustness-efficiency trade-off. On one hand, it remains consistent in the presence of label noise. On the other hand, it is more efficient than  $k$ NN, SVM and even LDA across all simulation settings, including noiseless settings.

**4.2.1 Experimental design.** Following Cannings, Fan and Samworth [10], we generate data from two models:

**M1**  $\mathbb{P}(Y = 1) = 0.9$  with  $X|Y = r \sim \mathcal{N}_5(\mu_r, I)$ , where  $\mu_1 = (3/2, 0, \dots, 0)^\top = -\mu_0$ .

**M2**  $X \sim U([0, 1]^5)$  with  $\mathbb{P}(Y = 1|X = x) = \min\{4(x_1 - 1/2)^2 + 4(x_2 - 1/2)^2, 1\}$ .

For each model, we generate an IID sample of size  $n + 10^4$ , reserving the first  $n$  observations for training and the remaining  $10^4$  for testing. For the training set, we set  $\rho \in \{0.1, \dots, 0.4\}$ . The optimal Bayes classifier minimizes this risk:  $C^{\text{Bayes}}(x) = \mathbb{1}(\eta(x) > 0.5)$ , where  $\eta(x) = \mathbb{P}(Y = 1|X = x)$ . For any classifier  $C'$ , we define its excess risk as  $R(C') - R(C^{\text{Bayes}})$ .

We compare three classifiers: Bayes,  $k$ -NN, LDA, and TabPFN. For each training dataset, each classifier trained on two versions of the data: a clean training set and a noise-corrupted version, hence yielding a total of six classification models to be evaluated. Details such as hyper-parameter selection are deferred to Appendix F. This process is repeated 1000 times, with Figure 6 showing the average excess risk across repetitions.

TABLE 5  
 $n = 500$ , beta-type I, orthogonal design (simple linear regression)

SNR	$s$	TabPFN				LASSO				SCAD				MCP				
		Relevant		Irrelevant		Relevant		Irrelevant		Relevant		Irrelevant		Relevant		Irrelevant		
		Bias <sup>2</sup>	Var															
1.22	1	0.0000	0.0012	0.0000	0.0000	0.0058	0.0016	0.0000	0.0000	0.0000	0.0012	0.0000	0.0000	0.0000	0.0012	0.0000	0.0000	0.0000
	5	0.0004	0.0081	0.0000	0.0004	0.0172	0.0085	0.0000	0.0006	0.0001	0.0077	0.0000	0.0001	0.0001	0.0077	0.0000	0.0000	0.0002
	10	0.0028	0.0196	0.0000	0.0025	0.0244	0.0174	0.0000	0.0020	0.0002	0.0180	0.0000	0.0007	0.0002	0.0179	0.0000	0.0007	0.0007
	20	0.0175	0.0500	0.0004	0.0099	0.0303	0.0360	0.0001	0.0079	0.0005	0.0400	0.0001	0.0051	0.0005	0.0407	0.0001	0.0049	0.0049
	30	0.0387	0.0783	0.0018	0.0177	0.0301	0.0579	0.0002	0.0166	0.0011	0.0707	0.0002	0.0146	0.0011	0.0719	0.0002	0.0142	0.0142
6	1	0.0000	0.0003	0.0000	0.0000	0.0022	0.0002	0.0000	0.0000	0.0000	0.0002	0.0000	0.0000	0.0000	0.0002	0.0000	0.0000	0.0000
	5	0.0000	0.0016	0.0000	0.0001	0.0038	0.0017	0.0000	0.0001	0.0000	0.0015	0.0000	0.0000	0.0000	0.0016	0.0000	0.0000	0.0000
	10	0.0004	0.0037	0.0000	0.0006	0.0053	0.0035	0.0000	0.0004	0.0000	0.0033	0.0000	0.0001	0.0000	0.0033	0.0000	0.0001	0.0001
	20	0.0022	0.0089	0.0001	0.0028	0.0070	0.0073	0.0000	0.0014	0.0001	0.0067	0.0000	0.0002	0.0001	0.0067	0.0000	0.0002	0.0002
	30	0.0055	0.0168	0.0003	0.0061	0.0079	0.0116	0.0000	0.0027	0.0001	0.0110	0.0000	0.0004	0.0001	0.0110	0.0000	0.0004	0.0004

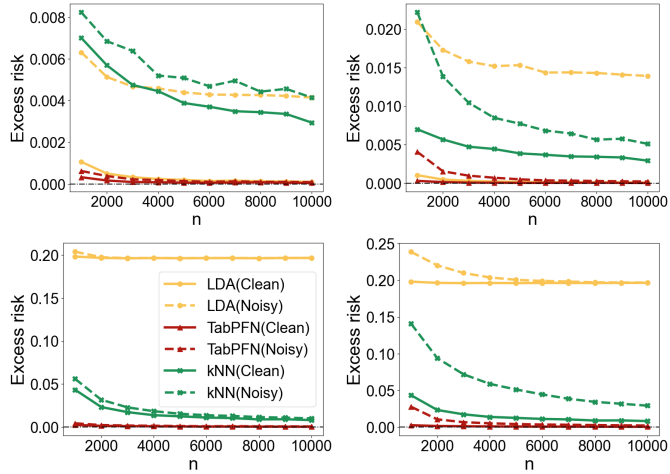


Fig 6: Excess risks under Model M1 (top row) and Model M2 (bottom row). The left column shows results for  $\rho = 0.1$ , while the right column presents results for  $\rho = 0.3$ .

**4.2.2 Prediction performance comparison.** Under both generative models, TabPFN (clean) performs as well as the optimal Bayes classifier when the training set size is bigger than 2K. TabPFN (noisy) shows slightly worse performance than its clean-data counterpart but demonstrates exceptional robustness to label noise in all cases while maintaining high accuracy. Even with noise levels as high as  $\rho = 0.3$ , TabPFN (noisy) nearly matches the optimal classifier given a sufficiently large training set ( $\geq 5K$  samples). LDA exhibits no robustness under M1 and performs poorly under M2 due to the nonlinear Bayes decision boundary. While the  $k$ -NN classifier shows some consistency—particularly under M2 with low noise levels—it is less robust than TabPFN in other scenarios. Moreover, Figure 7 demonstrates that TabPFN remains robust even at  $\rho = 0.4$  for small training set sizes.

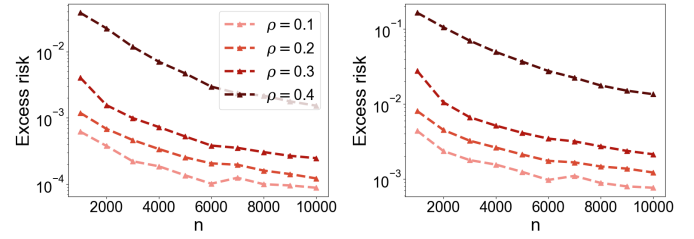


Fig 7: TabPFN (noisy) excess risk for varying  $\rho$  values under M1 (left) and M2 (right).

## 5. DISCUSSION

### 5.1 Foundation models

In 2021, Bommasani et al. [7] coined the term “foundation model” to refer to “any model that is trained on broad data (generally using self-supervision at scale) that can be adapted (e.g., fine-tuned) to a wide range of downstream tasks”. They also noted a paradigm shift in artificial intelligence which de-prioritized the development of task-specific models in favor of building these foundation models, with LLMs being the most prominent examples. Until recently, the modality of tabular data has resisted this trend, but the tide may be turning. Hollmann et al. [30] provided a proof-of-concept that, in addition to regression and classification, TabPFN can support “data generation, density estimation, learning reusable embeddings and fine-tuning”, consequently claiming that TabPFN is a tabular foundation model.<sup>10</sup> Our investigations support this claim by showing that simple applications of TabPFN can surpass state-of-the-art approaches to some statistical problems.

These studies are of course preliminary and we do not suggest that TabPFN is a perfect model—it seems to struggle with dense regression, cannot handle  $\geq 500$

<sup>10</sup>These capabilities were not fully investigated by Hollmann et al. [30] and some are not supported by their publicly available code at the time of writing.

features, and has MSE curves which seem to plateau for  $n \geq 10K$  samples [38]. On the other hand, the evidence suggests that tabular foundation models are not only possible, but have the potential to reshape how a wide range of statistical tasks are approached. In addition, Van Breugel and Van Der Schaar [52] have a bold vision of tabular foundational models being able to perform automatic meta-analyses, out-of-domain simulation, and other tasks for which adequate methodology does not yet exist. This line of thinking—that there may one day be *one model to rule them all*—is of course contrary to mainstream statistical thinking, which has traditionally emphasized bespoke models for different problems. Just as AI scientists wrestle with the academic and societal consequences of foundation models, statisticians may also be forced to confront profound changes in our field.

## 5.2 In-context learning

Another way in which TabPFN challenges current statistical thinking is via its illustration of the power of “in-context learning”, whose historical development we now discuss. In a landmark paper, Brown et al. [9] studied the LLM GPT-3 and discovered that it could learn how to perform tasks (e.g., language translation) that it was not explicitly trained to do and without changing any of the model’s parameters, simply by providing examples of the task in a prompt (text input) to the model. They called this ability “in-context learning” (ICL). Garg et al. [22] later framed ICL as a statistical learning problem. Under their framework, a prompt  $P$  is a random sequence  $(X_1, f(X_1), \dots, X_n, f(X_n), X_{n+1})$ , where  $X_1, \dots, X_{n+1}$  are drawn IID from a covariate distribution  $D_X$  and  $f$  is drawn from a distribution  $D_f$  over a function class  $\mathcal{F}$ . A model  $M$  is a fixed mapping from prompts to the (real-valued) label space and is said to have learned  $\mathcal{F}$  in-context (with respect to  $(D_X, D_f)$ ) if  $\mathbb{E}_P[l(M(P), f(X_{n+1}))] \leq \epsilon$  for some tolerance  $\epsilon$  and loss function  $l$ . Garg et al. [22] was able to show via numerical experiments that a transformer, trained from scratch on IID prompts generated as described above, could successfully learn simple function classes (e.g. linear functions) in-context, inspiring a wave of theoretical interest in the problem (see for instance Bai et al. [5], Kim, Nakamaki and Suzuki [33], Zhang, Frei and Bartlett [57]).

On the other hand, it seems that Brown et al. [9] and Garg et al. [22]’s definitions of ICL are respectively too broad and too narrow to capture the scope of the learning strategy employed by TabPFN and other recent work claiming to implement ICL to solve statistical estimation problems. These include causal discovery [15], posterior inference for generalized linear

models, factor models, and Gaussian mixture models [45], RNA folding time density estimation [48], and Poisson mean estimation under empirical Bayes [50]. None of these works provide a definition of ICL, but we find that the common denominator is that they *train a transformer model using a large number of synthetic datasets to learn a mapping on the space of datasets*. The target of the mapping can be a causal graph, a posterior distribution on parameter vector, or a Poisson mean vector estimate. In each problem, the ICL approach achieves higher accuracy than SOTA methods, such as variational inference for posterior approximation, or non-parametric maximum-likelihood estimation in the case of empirical Bayes.

## 5.3 Future directions

These advances present both opportunities and challenges for the statistical community. TabPFN’s success stems from a synthesis of ideas across disciplines, coupled with non-trivial engineering efforts. The current version [30] builds on its predecessor [29], with key improvements in (1) prior data generation and (2) transformer architecture—both empirically shown to enhance performance. As statisticians, we can contribute to this evolving field by addressing critical questions:

- **Interpretability & theoretical foundations:** Transformers, with millions of parameters, often lack interpretability. Understanding when TabPFN succeeds or fails—along with its statistical guarantees—remains an open problem.
- **Reliability in practice:** While TabPFN and related methods show promise as off-the-shelf tools for biomedical and other applications, their real-world reliability—particularly for inference tasks—requires rigorous evaluation.
- **Scalability & limitations:** Current implementations struggle with dense/high-dimensional regression and  $> 10K$  samples. Addressing this bottleneck is essential for broader applicability. Recent work [25, 44] offers preliminary solutions, but fundamental constraints remain.

## REFERENCES

- [1] ANGELOPOULOS, A. N., BATES, S., FANNJIANG, C., JORDAN, M. I. and ZRNIC, T. (2023). Prediction-powered inference. *Science* **382** 669–674.
- [2] APLEY, D. W. and ZHU, J. (2020). Visualizing the effects of predictor variables in black box supervised learning models. *Journal of the Royal Statistical Society Series B: Statistical Methodology* **82** 1059–1086.
- [3] ATHEY, S., TIBSHIRANI, J. and WAGER, S. (2019). Generalized random forests. *The Annals of Statistics* **47** 1148 – 1178. <https://doi.org/10.1214/18-AOS1709>
- [4] AZRIEL, D., BROWN, L. D., SKLAR, M., BERK, R., BUJA, A. and ZHAO, L. (2022). Semi-supervised linear regression. *Journal of the American Statistical Association* **117** 2238–2251.

[5] BAI, Y., CHEN, F., WANG, H., XIONG, C. and MEI, S. (2023). Transformers as statisticians: provable in-context learning with in-context algorithm selection. *Advances in Neural Information Processing Systems* **36** 57125–57211.

[6] BATTOCCHI, K., DILLON, E., HEI, M., LEWIS, G., OKA, P., OPRESCU, M. and SYRGKANIS, V. (2019). EconML: a Python package for ML-based heterogeneous treatment effects estimation. <https://github.com/pywhy/EconML>. Version 0.x.

[7] BOMMASANI, R., HUDSON, D. A., ADELI, E., ALTMAN, R., ARORA, S., VON ARX, S., BERNSTEIN, M. S., BOHG, J., BOSSELUT, A., BRUNSKILL, E. et al. (2021). On the opportunities and risks of foundation models. *arXiv preprint arXiv:2108.07258*.

[8] BROOKS-GUNN, J., LIAW, F.-R. and KLEBANOV, P. K. (1992). Effects of early intervention on cognitive function of low birth weight preterm infants. *The Journal of Pediatrics* **120** 350–359.

[9] BROWN, T., MANN, B., RYDER, N., SUBBIAH, M., KAPLAN, J. D., DHARIWAL, P., NEELAKANTAN, A., SHYAM, P., SASTRY, G., ASKELL, A. et al. (2020). Language models are few-shot learners. *Advances in Neural Information Processing Systems* **33** 1877–1901.

[10] CANNINGS, T. I., FAN, Y. and SAMWORTH, R. J. (2020). Classification with imperfect training labels. *Biometrika* **107** 311–330.

[11] CARUANA, R., KARAMPATZIAKIS, N. and YESSENALINA, A. (2008). An empirical evaluation of supervised learning in high dimensions. In *Proceedings of the 25th International Conference on Machine learning* 96–103.

[12] CHAKRABORTTY, A. and CAI, T. (2018). Efficient and adaptive linear regression in semi-supervised settings. *The Annals of Statistics* **46** 1541 – 1572.

[13] CHIPMAN, H. A., GEORGE, E. I. and MCCULLOCH, R. E. (2010). BART: Bayesian additive regression trees. *The Annals of Applied Statistics* **4** 266–298.

[14] COYLE, J. R., HEJAZI, N. S., MALENICA, I., PHILLIPS, R. V., ARNOLD, B. F., MERTENS, A., BENJAMIN-CHUNG, J., CAI, W., DAYAL, S., COLFORD JR, J. M. et al. (2020). Targeting learning: robust statistics for reproducible research. *arXiv preprint arXiv:2006.07333*.

[15] DHIR, A., ASHMAN, M., REQUEIMA, J. and VAN DER WILK, M. (2025). A meta-learning approach to Bayesian causal discovery. In *The Thirteenth International Conference on Learning Representations*.

[16] DONOHO, D. L. and JOHNSTONE, I. M. (1995). Adapting to Unknown Smoothness via Wavelet Shrinkage. *Journal of the American Statistical Association* **90** 1200–1224. <https://doi.org/10.1080/01621459.1995.10476626>

[17] DORIE, V., HILL, J., SHALIT, U., SCOTT, M. and CERVONE, D. (2019). Automated versus Do-It-Yourself Methods for Causal Inference: Lessons Learned from a Data Analysis Competition. *Statistical Science* **34** 43 – 68.

[18] ERICKSON, N., PURUCKER, L., TSCHALZEV, A., HOLZMÜLLER, D., DESAI, P. M., SALINAS, D. and HUTTER, F. (2025). TabArena: A living benchmark for machine learning on tabular data. *arXiv preprint arXiv:2506.16791*.

[19] FERNÁNDEZ-DELGADO, M., CERNADAS, E., BARRO, S. and AMORIM, D. (2014). Do we need hundreds of classifiers to solve real world classification problems? *The Journal of Machine Learning Research* **15** 3133–3181.

[20] FEURER, M., VAN RIJN, J. N., KADRA, A., GIJSBERS, P., MALLIK, N., RAVI, S., MÜLLER, A., VANSCHOREN, J. and HUTTER, F. (2021). Openml-python: an extensible python api for openml. *Journal of Machine Learning Research* **22** 1–5.

[21] FOSTER, D. J. and SYRGKANIS, V. (2023). Orthogonal statistical learning. *The Annals of Statistics* **51** 879–908.

[22] GARG, S., TSIPRAS, D., LIANG, P. S. and VALIANT, G. (2022). What can transformers learn in-context? a case study of simple function classes. *Advances in Neural Information Processing Systems* **35** 30583–30598.

[23] GARNELO, M., SCHWARZ, J., ROSENBAUM, D., VIOLA, F., REZENDE, D. J., ESLAMI, S. and TEH, Y. W. (2018). Neural processes. *arXiv preprint arXiv:1807.01622*.

[24] GRINSZTAJN, L., OYALLON, E. and VAROQUAUX, G. (2022). Why do tree-based models still outperform deep learning on typical tabular data? *Advances in Neural Information Processing Systems* **35** 507–520.

[25] GRINSZTAJN, L., FLÖGE, K., KEY, O., BIRKEL, F., JUND, P., ROOF, B., JÄGER, B., SAFARIC, D., ALESSI, S., HAYLER, A. et al. (2025). TabPFN-2.5: Advancing the State of the Art in Tabular Foundation Models. *arXiv preprint arXiv:2511.08667*.

[26] HAHN, P. R., DORIE, V. and MURRAY, J. S. (2019). Atlantic causal inference conference (acic) data analysis challenge 2017. *arXiv preprint arXiv:1905.09515*.

[27] HAHN, P. R., MURRAY, J. S. and CARVALHO, C. M. (2020). Bayesian Regression Tree Models for Causal Inference: Regularization, Confounding, and Heterogeneous Effects (with Discussion). *Bayesian Analysis* **15** 965 – 2020. <https://doi.org/10.1214/19-BA1195>

[28] HASTIE, T., TIBSHIRANI, R. and TIBSHIRANI, R. (2020). Best subset, forward stepwise or lasso? Analysis and recommendations based on extensive comparisons. *Statistical Science* **35** 579–592.

[29] HOLLMANN, N., MÜLLER, S., EGGENSPERGER, K. and HUTTER, F. (2022). TabPFN: a transformer that solves small tabular classification problems in a second. In *NeurIPS 2022 First Table Representation Workshop*.

[30] HOLLMANN, N., MÜLLER, S., PURUCKER, L., KRISHNAKUMAR, A., KÖRFER, M., HOO, S. B., SCHIRRMESTER, R. T. and HUTTER, F. (2025). Accurate predictions on small data with a tabular foundation model. *Nature* **637** 319–326.

[31] KAWAKITA, M. and KANAMORI, T. (2013). Semi-supervised learning with density-ratio estimation. *Machine Learning* **91** 189–209.

[32] KENNEDY, E. H. (2023). Towards optimal doubly robust estimation of heterogeneous causal effects. *Electronic Journal of Statistics* **17** 3008 – 3049.

[33] KIM, J., NAKAMAKI, T. and SUZUKI, T. (2024). Transformers are minimax optimal nonparametric in-context learners. *Advances in Neural Information Processing Systems* **37** 106667–106713.

[34] KÜNZEL, S. R., SEKHON, J. S., BICKEL, P. J. and YU, B. (2019). Metalearners for estimating heterogeneous treatment effects using machine learning. *Proceedings of the National Academy of Sciences* **116** 4156–4165.

[35] LEPSKII, O. V. (1991). On a Problem of Adaptive Estimation in Gaussian White Noise. *Theory of Probability & Its Applications* **35** 454–466. <https://doi.org/10.1137/1135065>

[36] MA, C., PATHAK, R. and WAINWRIGHT, M. J. (2023). Optimally tackling covariate shift in RKHS-based nonparametric

metric regression. *The Annals of Statistics* **51** 738 – 761. <https://doi.org/10.1214/23-AOS2268>

[37] MÜLLER, S., HOLLMANN, N., ARANGO, S. P., GRABOCKA, J. and HUTTER, F. (2022). Transformers can do Bayesian inference. In *International Conference on Learning Representations*.

[38] NAGLER, T. (2023). Statistical foundations of prior-data fitted networks. In *Proceedings of the 40th International Conference on Machine Learning. Proceedings of Machine Learning Research* **202** 25660–25676. PMLR.

[39] NIE, X. and WAGER, S. (2020). Quasi-oracle estimation of heterogeneous treatment effects. *Biometrika* **108** 299–319.

[40] OLSON, R. S., CAVA, W. L., MUSTAHSAN, Z., VARIK, A. and MOORE, J. H. (2018). Data-driven advice for applying machine learning to bioinformatics problems. In *Biocomputing 2018: Proceedings of the Pacific Symposium* 192–203. World Scientific.

[41] PEARL, J. (2009). *Causality*. Cambridge university press.

[42] QIN, J., LIU, Y., LI, M. and AND, C.-Y. H. (2025). Distribution-free prediction intervals under covariate shift, with an application to causal inference. *Journal of the American Statistical Association* **120** 559–571.

[43] QIU, H., DOBRIBAN, E. and TCHELEGAN, E. (2023). Prediction sets adaptive to unknown covariate shift. *Journal of the Royal Statistical Society Series B: Statistical Methodology* **85** 1680–1705.

[44] QU, J., HOLZMÜLLER, D., VAROQUAUX, G. and MORVAN, M. L. (2025). TabICL: a tabular foundation model for in-context learning on large data. *arXiv preprint arXiv:2502.05564*.

[45] REUTER, A., RUDNER, T. G., FORTUIN, V. and RÜGAMER, D. (2025). Can transformers learn full Bayesian inference in context? *arXiv preprint arXiv:2501.16825*.

[46] RUBIN, D. B. (1974). Estimating causal effects of treatments in randomized and nonrandomized studies. *Journal of Educational Psychology* **66** 688.

[47] RUBIN, D. B. (1987). *Multiple Imputation for Nonresponse in Surveys. Wiley Series in Probability and Statistics*. John Wiley & Sons, Inc., New York, NY, USA. <https://doi.org/10.1002/9780470316696>

[48] SCHEUER, D., RUNGE, F., FRANKE, J. K. H., WOLFINGER, M. T., FLAMM, C. and HUTTER, F. (2025). KinPFN: Bayesian approximation of RNA folding kinetics using prior-data fitted networks. In *The Thirteenth International Conference on Learning Representations*.

[49] SONG, S., LIN, Y. and ZHOU, Y. (2024). A general M-estimation theory in semi-supervised framework. *Journal of the American Statistical Association* **119** 1065–1075.

[50] TEH, A., JABBOUR, M. and POLYANSKIY, Y. (2025). Solving empirical Bayes via transformers. *arXiv preprint arXiv:2502.09844*.

[51] TIBSHIRANI, R. J., FOYgel BARBER, R., CANDES, E. and RAMDAS, A. (2019). Conformal prediction under covariate shift. *Advances in neural information processing systems* **32**.

[52] VAN BREUGEL, B. and VAN DER SCHAAR, M. (2024). Position: why tabular foundation models should be a research priority. In *Proceedings of the 41st International Conference on Machine Learning. Proceedings of Machine Learning Research* **235** 48976–48993. PMLR.

[53] VASWANI, A., SHAZER, N., PARMAR, N., USZKOREIT, J., JONES, L., GOMEZ, A. N., KAISER, L. and POLOSUKHIN, I. (2017). Attention is all you need. *Advances in Neural Information Processing Systems* **30**.

[54] WANG, K. (2025). Pseudo-labeling for kernel ridge regression under covariate shift. *The Annals of Statistics to appear*.

[55] WANG, C., WU, Q., WEIMER, M. and ZHU, E. (2021). FLAML: a fast and lightweight automl library. *Proceedings of Machine Learning and Systems* **3** 434–447.

[56] YANG, Y., KUCHIBHOTLA, A. K. and TCHELEGAN, E. (2024). Doubly robust calibration of prediction sets under covariate shift. *Journal of the Royal Statistical Society Series B: Statistical Methodology* **86** 943–965.

[57] ZHANG, R., FREI, S. and BARTLETT, P. L. (2024). Trained transformers learn linear models in-context. *Journal of Machine Learning Research* **25** 1–55.

[58] ZHU, X. (2010). *Semi-supervised learning*. In *Encyclopedia of Machine Learning* 892–897. Springer US, Boston, MA.

## APPENDIX A: EXPERIMENT DETAILS FOR STUDY I

We adopt the same experimental setup as in Song, Lin and Zhou [49]. For completeness, we detail the simulation settings in Section A.1 and present additional results in Section A.2.

### A.1 Simulation settings

In correspondence with the three settings in Table 6, we describe the data-generating model for each setting respectively.

- **Linear regression working model.** In this setting, the data is generated from

$$Y = \alpha_0 + \alpha_1^\top X + \alpha_2^\top [X^3 - X^2 + \exp(X)] + \epsilon,$$

where  $X \sim \mathcal{N}_p(0, I)$  and  $\epsilon \sim \mathcal{N}(0, 4)$ . The power and exponential operations on the vector  $X$  are performed element-wise. We let  $\alpha_0 = 1$ , with  $\alpha_1$  and  $\alpha_2$  both being all-ones vectors.

- **Logistic regression working model.** In this setting, the data is generated from

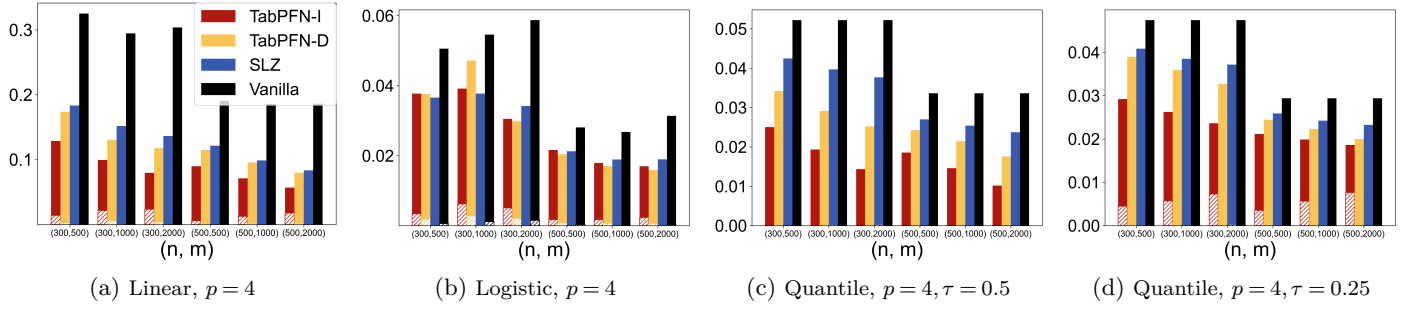
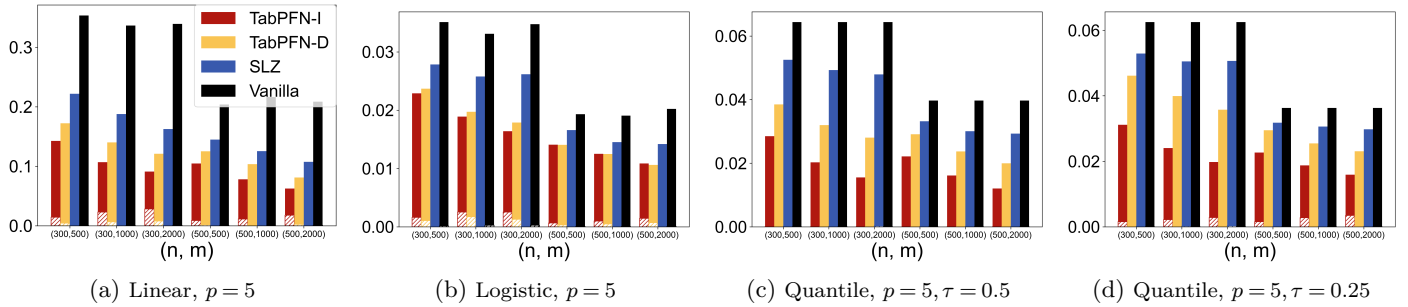
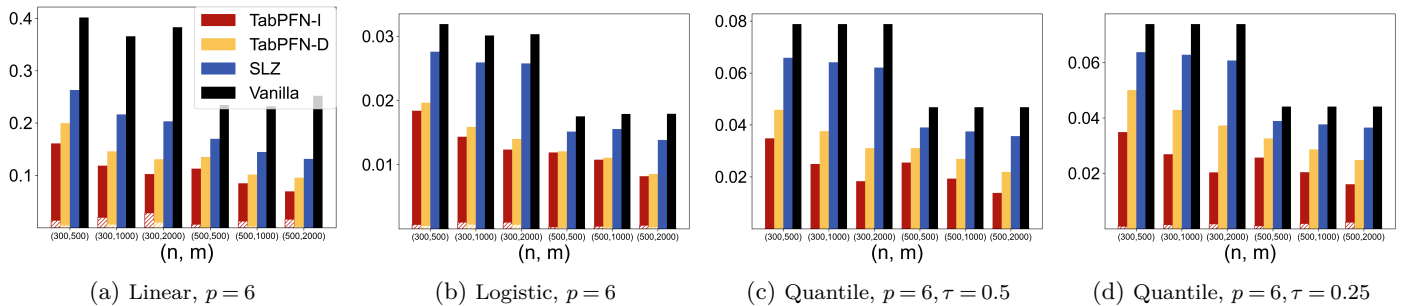
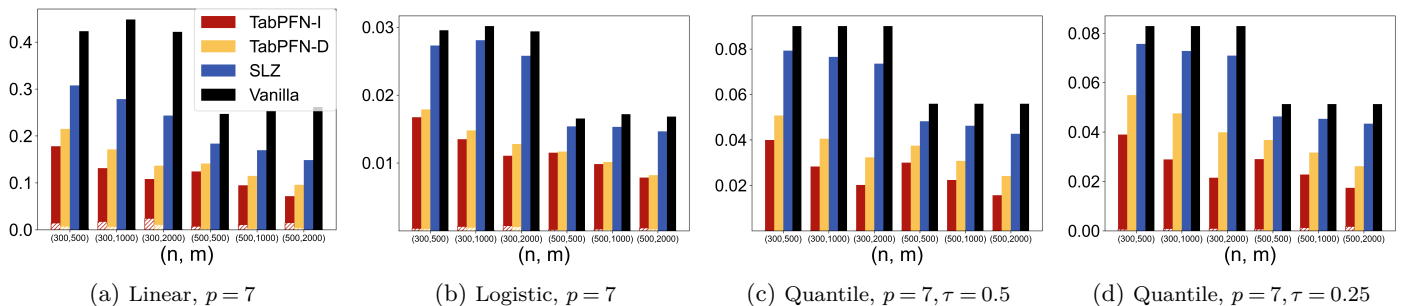
$$\mathbb{P}(Y = 1 | X) = [1 + \exp(-\alpha_0 - \alpha_1^\top X - \alpha_2^\top X^2)]^{-1},$$

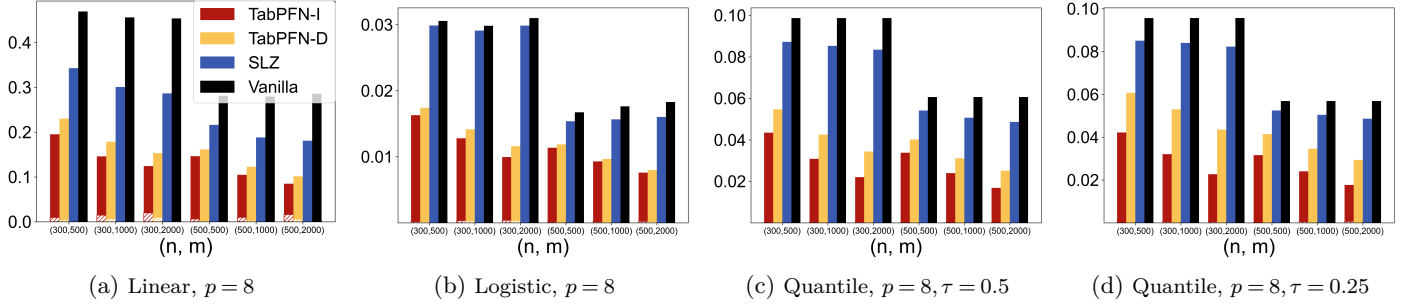
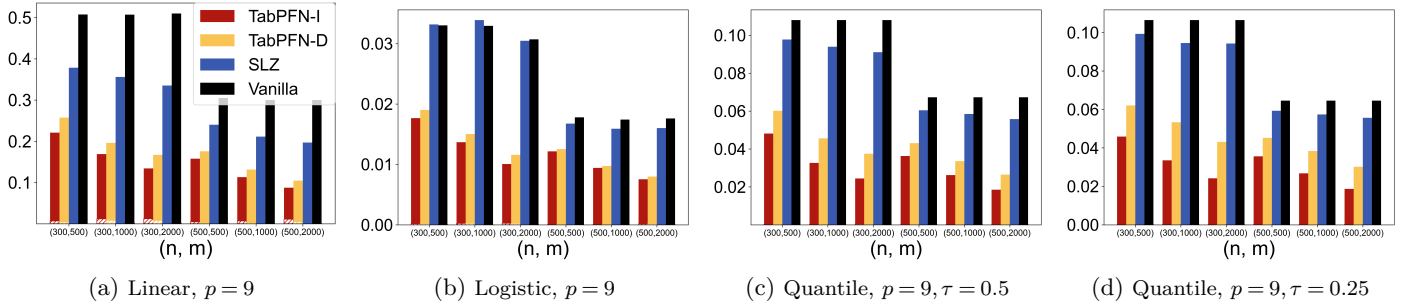
where  $X \sim 0.5\mathcal{N}_p(1, \Sigma) + 0.5\mathcal{N}_p(-1, \Sigma)$ , and  $\Sigma$  is a matrix with  $(i, j)$ -th entry equal to  $0.5^{|i-j|}$ . We set  $\alpha_0 = 11$ ,  $\alpha_1$  as a vector of all 1s, and  $\alpha_2$  as a vector of all  $-1$ s.

- **Linear quantile regression working model.** In this setting, the data is generated from

$$Y = \alpha_0 + \alpha_1^\top X + \alpha_2 \sum_{j,k} x_j x_k + (1 + \alpha_3^\top X)\epsilon,$$

where  $X \sim \mathcal{N}_p(0, I)$ , and  $\epsilon \sim \mathcal{N}(0, 1)$ . We set  $\alpha_0 = \alpha_2 = 1$ ,  $\alpha_1 = 0.5\mathbf{1}_p$ , and  $\alpha_3 = (0.5\mathbf{1}_{p-\lfloor p/2 \rfloor}, \mathbf{0}_{\lfloor p/2 \rfloor})$ , where  $\mathbf{1}_d$  and  $\mathbf{0}_d$  denote  $d$ -dimensional all-ones and all-zeros vectors, respectively.

Fig 8: MSE and bias results for  $p = 4$  for the semi-supervised settings.Fig 9: MSE and bias results for  $p = 5$  for the semi-supervised settings.Fig 10: MSE and bias results for  $p = 6$  for the semi-supervised settings.Fig 11: MSE and bias results for  $p = 7$  for the semi-supervised settings.

Fig 12: MSE and bias results for  $p = 8$  for the semi-supervised settings.Fig 13: MSE and bias results for  $p = 9$  for the semi-supervised settings.

## A.2 Additional simulation results

We include all the simulation results in Figures 8 to 13. With the sole exception of the  $p = 4$  case under logistic regression, TabPFN-I consistently outperforms all competing methods.

## A.3 Real data comparison

The datasets are obtained from OpenML. We used the dataset search interface at [www.openml.org/](http://www.openml.org/), selecting datasets with fewer than 10 features and more than 1,000 instances, and verified that all features are numerical. We then downloaded datasets from the top of this filtered list. The restriction to fewer than 10 features is imposed because the SLZ implementation can exhibit numerical instability when the dimensionality is large. The requirement of a sufficiently large number of instances ensures that the oracle estimator provides a reasonable approximation to the true parameter values. To maintain computational efficiency, we further restricted datasets to have fewer than 50,000 instances. Even after this filtering, we occasionally encountered matrix-inversion issues in the SLZ implementation; when such cases occurred, we skipped the problematic dataset and selected the next one on the list. This leads to the following datasets for regression and classification respectively:

- **Regression:** kin8nm (ID:189), house\_8L (ID: 218), puma8NH (ID: 225), BNG (stock) (ID: 1200), cmc (ID: 45052)
- **Classification:** BNG(breast-w) (ID:251), kin8nm (ID:807), puma8NH (ID: 816), mozilla4 (ID: 1046), wilt (ID: 40983)

## APPENDIX B: EXPERIMENT DETAILS FOR STUDY II

We provide the details for the causal inference experiment and the full experiment result in this section.

### B.1 Simulation settings and additional results

The specification of the feature distribution, propensity function, base function, and treatment effect function under all setups are given in Table 6. These functions corresponding to the following setting:

- **Setup A:** complicated  $e(x)$  and  $b(x)$ , but a relatively simple  $\tau(x)$ .
- **Setup B:** randomized trial with a complex  $b(x)$  and  $\tau(x)$ .
- **Setup C:** complex  $e(x)$  and  $b(x)$ , but a constant  $\tau(x)$ .
- **Setup D:** response under treatment is independent of the response under control, and hence there is no statistical benefit of jointly learning the two responses.

TABLE 6  
Experimental setups with distributional and functional specifications

Setup	Propensity $e(X)$	Base $b(X)$	Effect $\tau(X)$
<b>A</b>	$\min\{0.8, \max\{\sin(\pi X_1 X_2), 0.2\}\}$	$\sin(\pi X_1 X_2) + 2(X_3 - .5)^2 + X_4 + .5X_5$	$.2 + (X_1 + X_2)/2$
<b>B</b>	.5	$\max\{0, X_1 + X_2, X_3\} + \max\{0, X_4 + X_5\}$	$X_1 + \log[1 + \exp(X_2)]$
<b>C</b>	$[1 + \exp(X_2 + X_3)]^{-1}$	$2 \log[1 + \exp(X_1 + X_2 + X_3)]$	1
<b>D</b>	$[1 + \exp(-X_1) + \exp(-X_2)]^{-1}$	$.5 \max\{0, X_1 + X_2 + X_3\} + .5 \max\{0, X_4 + X_5\}$	$\max\{0, X_1 + X_2 + X_3\} - \max\{0, X_4 + X_5\}$
<b>E</b>	$[1 + \exp(3X_2 + 3X_3)]^{-1}$	$5 \max\{0, X_1 + X_2\}$	$2 \max\{(X_1 > .1), (X_2 > .1)\} - 1$
<b>F</b>	$[1 + \exp(3X_2 + 3X_3)]^{-1}$	$5 \max\{0, X_1 + X_2\}$	$X_1 + \log[1 + \exp(X_2)]$

- **Setup E:** large  $b(x)$  resulting in substantial confounding, discontinuous  $\tau(x)$ .
- **Setup F:** similar to setup  $E$ , but with a smooth  $\tau(x)$ .

Our experiments are implemented using the *econml* [6] package in Python, we use the FLAML package [55] to implement all AutoML-based learners. We use the 5-fold cross-validation to choose the optimal algorithms and its corresponding hyperparameters for AutoML-based learners. We randomly generate data from each setting for 100 times and the average test MSE over 100 repetitions for CATE is reported in Table 7 and Table 8.

## B.2 Real data comparison

**Data.** The Infant Health and Development Program (IHDP) [8] dataset contains  $n = 4302$  subjects with 8 covariates capturing demographic, prenatal, and birth-related characteristics, a binary treatment indicating participation in a specialist early-childhood intervention program, and continuous outcomes representing cognitive test scores measured at age 3. We use a collection of semi-synthetic versions of the dataset that were created for the ACIC 2017 Causal Inference Benchmark challenge described in Hahn, Dorie and Murray [26], where treatment assignments and potential outcomes are simulated conditional on the real-world covariates. This design ensures access to the ground-truth treatment effects, allowing quantitative comparison across estimators via the MSE of the CATE. We accessed the data via Richard Hahn’s personal website: <https://math.la.asu.edu/~prhahn/>.

Each semi-synthetic dataset is generated according to one of 24 data-generating processes (DGPs) that were chosen to systematically vary structural and noise properties to probe robustness of causal estimators. Specifically, the DGPs are organized into three broad settings for the error structure:

- **IID:** Errors are generated independently across individuals, corresponding to the standard assumption of homogeneous, uncorrelated residuals.

- **Non-additive:** Treatment effects and outcomes are generated via nonlinear functions and interaction terms, inducing complex, non-additive response surfaces.
- **Group Corr:** The error terms include intra-group correlation components to mimic unobserved group-level dependencies (e.g., hospitals or study sites), introducing residual correlation beyond observed covariates and thereby violating the IID assumption.

A fourth error type, heteroskedastic case, was later discovered by Hahn, Dorie and Murray [26] to contain inconsistencies and hence omitted from the benchmark comparison.

Within each setting, eight distinct DGPs are defined to explore combinations of three factors that affect causal inference difficulty: the effect magnitude  $\xi$  (large vs. small), the noise level  $\eta$  (low vs. high), and the selection strength  $\kappa$  (weak vs. strong confounding). Overall, these yield 3 settings  $\times$  8 scenarios  $\times$  250 replications = 6,000 semi-synthetic datasets derived from the IHDP covariates.

**Evaluation.** We compare four TabPFN-based meta-learners (S-Learner, T-Learner, X-Learner, and DR-Learner) with the 22 estimators reported in the benchmark challenge. For a fair comparison, we only include methods with available results across all 6,000 datasets, resulting in 16 baseline approaches. For all TabPFN-based methods, we use the TabPFN classifier to estimate the propensity score model and the TabPFN regressor to fit the outcome model, as well as any auxiliary models with continuous responses. The evaluation protocol follows that of Hahn, Dorie and Murray [26], and we estimate the RMSE of the CATEs based on 250 repetitions under each scenario. The results for the baseline approaches were taken directly from Richard Hahn’s personal website and were not recalculated.

The comparison of different methods across the 24 scenarios is presented in Figure 14. TabPFN-based methods, especially X+PS and X learners shown strong performance in almost all scenarios.

TABLE 7

The median of test MSE of various CATE estimators over 100 repetitions setup A–C. The **smallest** test MSE is highlighted in boldface and the second smallest test MSE is highlighted with underline.

Setup	N	$\sigma^2$	DR		S		T		X		R	Oracle
			TabPFN	AutoML	TabPFN	AutoML	TabPFN	AutoML	TabPFN	AutoML	AutoML	AutoML
A	500	0.5	<b>0.0353</b>	0.0459	<b>0.0306</b>	0.0451	0.0904	0.2367	0.0445	0.0592	0.0423	0.0527
		1	<u>0.0491</u>	0.0720	<b>0.0393</b>	0.0537	0.1672	0.6091	0.0619	0.0920	0.0681	0.0803
		2	0.0701	0.2610	<u>0.0647</u>	<u>0.0666</u>	0.4703	1.6589	0.1520	0.2904	0.1776	0.2072
	1000	0.5	<u>0.0358</u>	0.0417	<b>0.0345</b>	0.0445	0.0603	0.1395	0.0379	0.0462	0.0408	0.0472
		1	<u>0.0360</u>	0.0519	<b>0.0298</b>	0.0513	0.1006	0.2939	0.0444	0.0651	0.0518	0.0559
		2	<b>0.0461</b>	0.0923	<u>0.0509</u>	0.0578	0.2419	0.8325	0.0864	0.1311	0.1145	0.1090
	2000	0.5	0.0379	0.0397	<b>0.0369</b>	0.0446	0.0545	0.0905	<u>0.0376</u>	0.0420	0.0399	0.0439
		1	<u>0.0360</u>	0.0412	<b>0.0308</b>	0.0468	0.0704	0.1536	0.0364	0.0467	0.0420	0.0473
		2	<u>0.0366</u>	0.0593	<b>0.0343</b>	0.0474	0.1390	0.4325	0.0499	0.0690	0.0628	0.0699
B	500	0.5	0.9449	0.9726	<b>0.8850</b>	<u>0.9161</u>	1.0594	1.2249	0.9615	1.0196	0.9670	0.9316
		1	0.9988	1.0338	<b>0.8487</b>	<u>0.9256</u>	1.2281	1.4780	1.0423	1.1467	1.0315	0.9917
		2	1.1678	1.5120	<b>0.8262</b>	<u>0.9279</u>	1.5869	2.4374	1.2474	1.3836	1.3388	1.2320
	1000	0.5	0.9236	0.9601	<b>0.8957</b>	<u>0.9283</u>	1.0003	1.0622	0.9317	0.9494	0.9633	0.9442
		1	0.9441	1.0354	<b>0.8731</b>	<u>0.9327</u>	1.0961	1.2457	0.9661	1.0426	0.9958	0.9811
		2	1.0131	1.2884	<b>0.8391</b>	<u>0.9405</u>	1.3271	1.4817	1.0791	1.1271	1.0919	1.1219
	2000	0.5	<u>0.9127</u>	0.9268	<b>0.9051</b>	0.9155	0.9776	1.0294	0.9240	0.9504	0.9263	0.9338
		1	<u>0.9136</u>	0.9475	<b>0.8938</b>	0.9226	1.0538	1.0820	0.9399	0.9784	0.9643	0.9552
		2	0.9298	1.0576	<b>0.8542</b>	0.9218	1.1856	1.2973	0.9940	1.0053	1.0489	1.1005
C	500	0.5	<b>0.9880</b>	1.1573	<u>1.0206</u>	1.1170	1.1092	1.6273	1.0315	1.1741	1.1283	1.0428
		1	<b>1.0148</b>	1.3708	<u>1.0550</u>	1.1556	1.3627	2.2214	1.1288	1.3321	1.2393	1.1755
		2	<u>1.2039</u>	2.0873	<b>1.1602</b>	1.1513	2.6658	3.5575	1.5984	1.6721	1.8985	1.5429
	1000	0.5	<b>0.9637</b>	1.0413	<u>1.0157</u>	1.0291	1.0450	1.3988	1.0100	1.1034	1.1083	1.0229
		1	<b>0.9460</b>	1.1973	<u>1.0287</u>	1.0447	1.1727	1.7895	1.0555	1.2451	1.1026	1.0677
		2	<b>0.9633</b>	1.4033	<u>1.0803</u>	1.1057	1.6611	2.6587	1.2487	1.3752	1.2119	1.1597
	2000	0.5	<b>0.9340</b>	1.0387	1.0003	1.0182	0.9863	1.1943	<u>0.9663</u>	1.0306	1.0254	0.9914
		1	<b>0.8782</b>	1.0625	0.9930	1.0291	1.0220	1.4187	<u>0.9542</u>	1.0955	1.0335	0.9766
		2	<b>0.7964</b>	1.1085	0.9754	1.0132	1.1751	1.9187	<u>0.9667</u>	1.1881	1.0689	1.0376

TABLE 8

The median of test MSE of various CATE estimators over 100 repetitions under setup D–F. The **smallest** test MSE is highlighted in boldface and the second smallest test MSE is highlighted with underline.

Setup	N	$\sigma^2$	DR		S		T		X		R	Oracle
			TabPFN	AutoML	TabPFN	AutoML	TabPFN	AutoML	TabPFN	AutoML	AutoML	AutoML
D	500	0.5	0.3146	0.3325	<b>0.3078</b>	0.3186	0.3194	0.3688	<u>0.3101</u>	0.3119	0.3297	0.3309
		1	<u>0.3234</u>	0.4091	<b>0.3104</b>	0.3252	0.3811	0.5066	0.3310	0.3577	0.3707	0.4057
		2	<u>0.3746</u>	0.6602	<b>0.3139</b>	0.3291	0.4476	0.8520	0.3796	0.4848	0.5620	0.6171
	1000	0.5	<u>0.3144</u>	0.3281	<b>0.3055</b>	0.3192	0.3033	0.3535	0.3087	0.3218	0.3204	0.3273
		1	0.3181	0.3387	<b>0.3093</b>	0.3224	0.3235	0.4137	<u>0.3149</u>	0.3412	0.3372	0.3445
		2	<u>0.3416</u>	0.4274	<b>0.3143</b>	0.3244	0.3837	0.5984	0.3433	0.4147	0.4255	0.4038
	2000	0.5	0.3199	0.3187	<b>0.3066</b>	0.3142	0.3108	0.3332	<u>0.3102</u>	0.3108	0.3139	0.3217
		1	0.3280	0.3294	<b>0.3058</b>	0.3153	0.3112	0.3492	<u>0.3086</u>	0.3234	0.3247	0.3297
		2	0.3601	0.3617	<b>0.3092</b>	0.3268	0.3708	0.4832	<u>0.3285</u>	0.3554	0.3702	0.3604
E	500	0.5	<b>0.9974</b>	1.1572	<u>1.0074</u>	1.1970	1.2127	1.9554	1.0603	1.2616	1.1245	1.3844
		1	<u>1.0197</u>	1.4416	<b>1.0125</b>	1.3366	1.5399	2.9947	1.1330	1.5996	1.2971	1.3954
		2	<u>1.1507</u>	1.9310	<b>1.0358</b>	1.4765	3.3103	6.6586	1.6092	2.5715	2.3374	2.1096
	1000	0.5	<b>0.9799</b>	1.0975	<u>1.0063</u>	1.1111	1.1177	1.4992	1.0463	1.1522	1.0671	1.3618
		1	<b>0.9830</b>	1.1957	<u>1.0086</u>	1.1500	1.2408	2.0187	1.0758	1.3126	1.1155	1.1570
		2	<u>1.0295</u>	1.4467	<b>1.0200</b>	1.2581	2.0002	3.9269	1.2779	1.7394	1.2873	1.4020
	2000	0.5	<b>0.9727</b>	1.0652	<u>1.0045</u>	1.1386	1.0880	1.3228	1.0290	1.0962	1.0190	2.5772
		1	<b>0.9612</b>	1.1088	<u>1.0018</u>	1.1134	1.1356	1.6436	1.0302	1.1732	1.0697	1.1482
		2	<b>0.9629</b>	1.2134	<u>0.9980</u>	1.1899	1.4940	2.7234	1.0977	1.4617	1.2380	1.1930
F	500	0.5	<b>0.9054</b>	1.1490	<u>0.9225</u>	1.1626	1.1541	2.1184	0.9731	1.2382	1.0686	2.2406
		1	<u>0.9285</u>	1.3720	<b>0.9276</b>	1.3698	1.4309	3.3303	1.0477	1.6814	1.3613	1.4709
		2	<u>1.0800</u>	2.2924	<b>0.9490</b>	1.5328	3.2448	7.4794	1.5656	2.4827	2.4312	1.8548
	1000	0.5	<b>0.8856</b>	1.0488	<u>0.9227</u>	1.0632	1.0674	1.5690	0.9577	1.0724	0.9831	4.0442
		1	<b>0.8831</b>	1.1311	<u>0.9259</u>	1.1132	1.1392	2.2563	0.9858	1.2539	1.0727	1.1675
		2	<b>0.9289</b>	1.5002	<u>0.9441</u>	1.2673	1.8699	4.3611	1.2044	1.7225	1.4343	1.4565
	2000	0.5	<b>0.8665</b>	0.9958	<u>0.9185</u>	1.0941	1.0345	1.2813	0.9315	1.0029	0.9412	5.4930
		1	<b>0.8353</b>	1.0804	<u>0.9139</u>	1.0236	1.0342	1.6587	0.9160	1.1017	0.9808	1.2046
		2	<b>0.8017</b>	1.2459	<u>0.9002</u>	1.1631	1.3191	2.8504	0.9575	1.3335	1.0868	1.1103

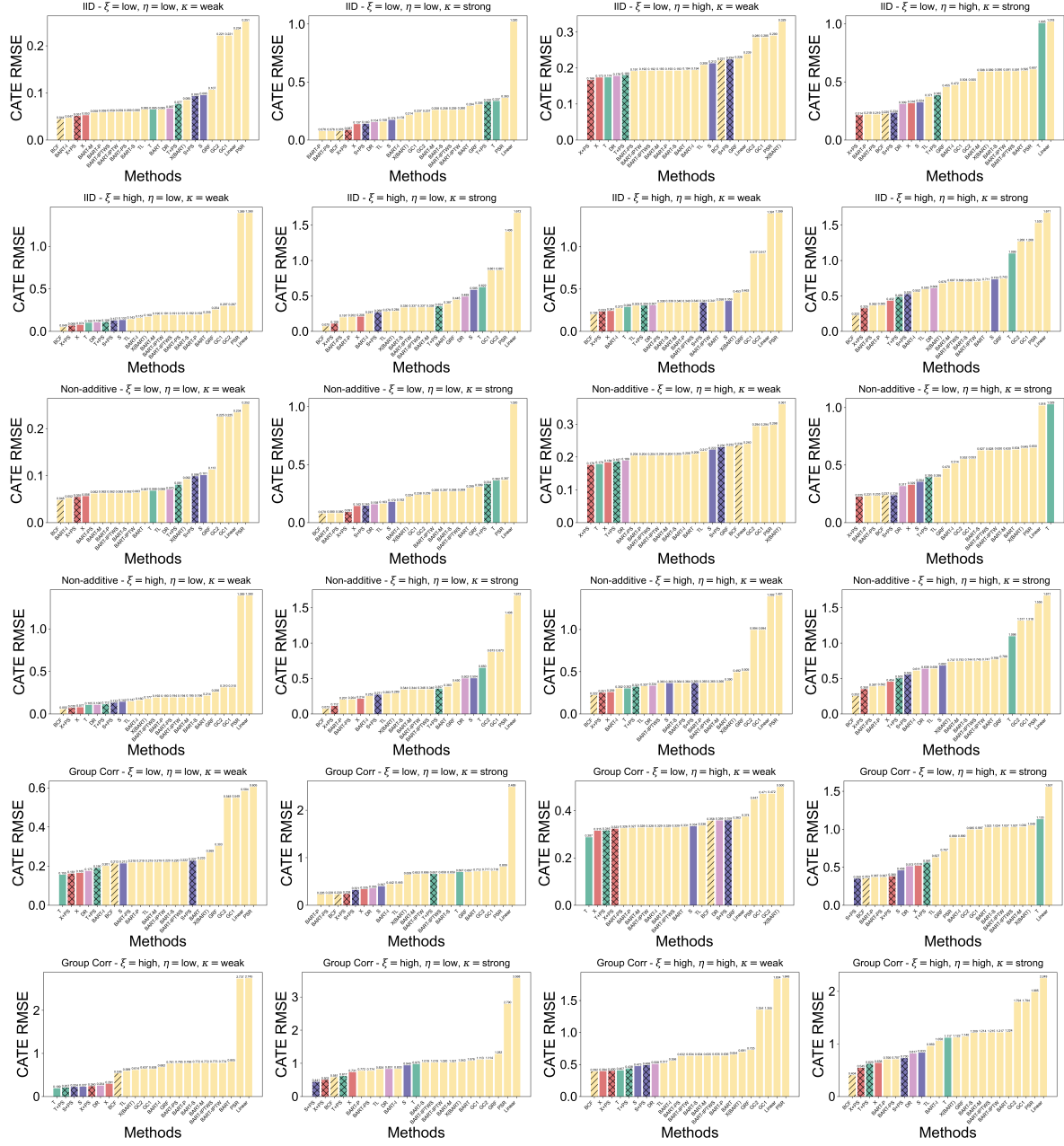


Fig 14: Performance comparison of TabPFN-based CATE estimators against SOTA methods on the ACIC 2017 benchmark. Results are shown across panels organized by error type, effect magnitude ( $\xi$ ), noise level ( $\eta$ ), and selection strength ( $\kappa$ ). Colored bars represent meta-learners built on TabPFN: **S-Learner**, **T-Learner**, **X-Learner**, **DR-Learner**, **S+PS-Learner**, **T+PS-Learner**, and **X+PS-Learner**. The **BCF** is shown for reference as the shaded yellow bar.

## APPENDIX C: EXPERIMENTAL DETAILS FOR STUDY III

### C.1 Additional simulation results

Figure 15 shows the Setting (ii) results, where the methods maintain their relative performance ordering observed in Setting (i).

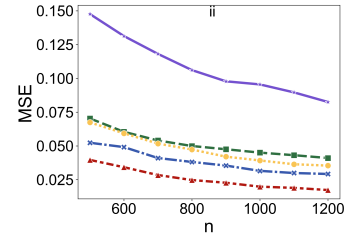


Fig 15: Covariate shift experiment under setting (ii).

## C.2 Real data comparison

**Airfoil Self-Noise Dataset.** The Airfoil dataset, used previously in studies on covariate shift [51], contains 1,503 observations with a five-dimensional covariate vector (*log frequency*, *angle of attack*, *chord length*, *free-stream velocity*, and *suction-side log displacement thickness*) and a continuous response variable  $Y$ . The data are randomly divided into training and testing subsets with a 7:3 ratio, that is, 70% of the observations are used for training and 30% for testing. To induce covariate shift, we follow the procedure in Tibshirani et al. [51]: we first split the data as described, and then resample the test set with replacement using importance weights

$$\omega(\mathbf{x}, y) = \exp(\mathbf{x}^T \boldsymbol{\beta}).$$

We consider two different shift settings characterized by

$$\boldsymbol{\beta}_1 = [-1, 1, -1, 1, -1]^T, \quad \boldsymbol{\beta}_2 = [-1, 0, 0, 0, 1]^T.$$

For each  $\boldsymbol{\beta}$  setting, the data splitting and resampling procedure is repeated ten times, and the mean squared prediction error (MSE) is averaged over the ten repetitions.

**Concrete Compressive Strength Dataset.** The Concrete dataset consists of 1,030 observations with an eight-dimensional covariate vector (*cement*, *blast furnace slag*, *fly ash*, *water*, *superplasticizer*, *coarse aggregate*, *fine aggregate*, and *age*) and the target variable is the measured compressive strength of concrete. As with the Airfoil data, the dataset is randomly split into 70% training and 30% testing observations. Covariate shift is then introduced by resampling the test set with replacement using

$$\omega(\mathbf{x}, y) = \exp(\mathbf{x}^T \boldsymbol{\beta}),$$

and we again consider two distinct settings:

$$\boldsymbol{\beta}_1 = [-1, 1, -1, 1, -1, 1, -1, 1]^T, \quad \boldsymbol{\beta}_2 = [-1, 0, 0, 0, 0, 0, 0, 1]^T.$$

Each  $\boldsymbol{\beta}$  setting is repeated for ten random data splits, and the average MSE is reported.

**Methods and Evaluation.** We compare the proposed TabPFN approach with several baseline methods (same as in the simulation study), including the naive gradient boosting regression, its importance-weighted variant, and the kernel ridge regression (KRR) methods from Wang [54]. Since the code in Wang [54] was limited to univariate  $X$ , we extend it to the multivariate case using a radial basis function (RBF) kernel. For each method and setting, the reported  $\pm$  values denote the *standard error* of the prediction mean squared error (PMSE) computed across the ten repetitions.

## APPENDIX D: COMPARISON WITH GAUSSIAN PROCESS REGRESSION

To study the adaptiveness of TabPFN, we evaluate the interpolation and extrapolation behavior of TabPFN trained on data sampled from predefined functions, comparing its performance to Gaussian process regression (GPR) as a baseline. Experiments are conducted in both one-dimensional (1D) and two-dimensional (2D) settings.

### D.1 Training data generation

**1D case.** The training set of size  $n$  consists of features  $x_i$  sampled uniformly over  $[-1, 1]$ . Responses are generated as:

$$y_i = f(x_i) + \epsilon_i, \quad \epsilon_i \stackrel{\text{i.i.d.}}{\sim} \mathcal{N}(0, 0.05^2),$$

where  $f$  is one of the following:

- (i) Linear function:  $f(x) = x$ ,
- (ii) Quadratic function:  $f(x) = x^2$ ,
- (iii) Step function:  $f(x) = \text{sign}(x)$  with  $\text{sign}(0) = 1$ ,
- (iv) A randomly generated piecewise-linear function with 4 pieces on  $[-1, 1]$ .

TabPFN is trained on this small dataset and prediction is made over the extended interval  $[-4, 4]$  to assess both interpolation ( $x \in [-1, 1]$ ) and extrapolation ( $x \notin [-1, 1]$ ) performance.

**2D case.** The training set consists of features  $\{(x_{i1}, x_{i2}) : i = 1, \dots, n\}$ , where  $x_{i1}$  and  $x_{i2}$  are each sampled uniformly from  $[-1, 1]$ . These points form a mesh grid, resulting in  $n^2$  total observations. We examine two cases:  $n = 11$  and  $n = 31$ . The responses are generated as:

$$y_i = f(x_{i1}, x_{i2}) + \epsilon_i, \quad \epsilon_i \stackrel{\text{i.i.d.}}{\sim} \mathcal{N}_2(0, 0.05^2 I),$$

where  $f$  is analogously defined as in the 1D case:

- (i) Linear function:  $f(x_1, x_2) = x_1 + x_2$ ,
- (ii) Quadratic function:  $f(x_1, x_2) = x_1^2 + x_2^2$ ,
- (iii) Step function:

$$f(x_1, x_2) = \begin{cases} -1, & \text{if } x_1 < 0 \text{ and } x_2 < 0, \\ 1, & \text{otherwise.} \end{cases}$$

- (iv) Piecewise-bilinear function. Given a 2D grid of randomly generated function values  $\{f_{ij}\}$  of size  $4^2$ . Uniformly divide  $[-1, 1]^2$  into  $4^2$  cells. For  $(x_1, x_2)$ , find which cell it falls into. Suppose it falls into the  $(i, j)$ th cell, compute the local coordinates:

$$x_{\text{loc},1} = 4x_1 - i, \quad x_{\text{loc},2} = 4x_2 - j.$$

and the bilinear function is given as

$$\begin{aligned} f(x_1, x_2) = & f_{i,j} \cdot (1 - x_{\text{loc},1})(1 - x_{\text{loc},2}) \\ & + f_{i+1,j} \cdot x_{\text{loc},1}(1 - x_{\text{loc},2}) \\ & + f_{i,j+1} \cdot (1 - x_{\text{loc},1})x_{\text{loc},2} \\ & + f_{i+1,j+1} \cdot x_{\text{loc},1}x_{\text{loc},2}. \end{aligned}$$

TabPFN is trained on this small dataset and prediction is made over the uniform mesh grid over  $[-4, 4]^2$  to assess both interpolation ( $x \in [-1, 1]^2$ ) and extrapolation ( $x \notin [-1, 1]^2$ ) performance.

## D.2 Baseline for comparison: Gaussian process regression

For both 1D and 2D cases, we compare TabPFN with Gaussian process regression (GPR). For Gaussian process regression, we consider 5 kernels: constant kernel  $\times$  RBF kernel, constant kernel  $\times$  Matern kernel, constant kernel  $\times$  RationalQuadratic kernel, constant kernel  $\times$  ExpSineSquared kernel, constant kernel  $\times$  RBF kernel + constant kernel  $\times$  Matern kernel. The candidate variance  $\sigma^2$  of the measurement error is over the grid  $[0.05, 0.1, 0.15, 0.2]$ . We maximize the marginal log-likelihood to select the optimal kernel and its corresponding optimal parameters, and the optimal measurement error variance. The GPR is implemented using the *GaussianProcessRegressor* in *scikit-learn* package in Python.

## D.3 Interpolation and extrapolation

The results for  $n = 31$  training data points are shown in Figure 16. The results when  $n = 11$  under 1D case are visualized in Figure 17. The results under 2D case are visualized in Figure 18.

We observe that in all cases, TabPFN fits a smoothly-varying curve that broadly resembles the GPR curve within the interpolation region. The notable differences are:

- Unlike GPR, TabPFN seems not to suffer from the Gibbs phenomenon (fluctuations at the point of discontinuity of a step function).
- TabPFN extrapolates at roughly the same level of the last observed response, whereas GPR quickly asymptotes to zero (the GPR prior mean).
- TabPFN is more conservative than GPR at fitting a quickly-varying function. GPR is able to roughly approximate the piecewise-linear function with  $n = 11$ , whereas TabPFN still outputs a constant model.
- TabPFN has a more diffuse conditional predictive distribution  $p(y|x)$  compared to GPR, especially away from the interpolation region.

## D.4 Uncertainty quantification

To assess the uncertainty quantification capability of TabPFN in comparison with GPR, we evaluate the predictive intervals of both methods in terms of their coverage ratio and interval length. For each predefined function, we generate 100 independent datasets following the data generation procedure described above. For each dataset, the model is trained on the corresponding training set and evaluated on a dense grid with a step size of 0.1 over the range  $[-4.5, 4.6]$ , which encompasses both the interpolation region ( $[-1, 1]$ ) and the extrapolation region ( $[-4.5, 4.6] \setminus [-1, 1]$ ). At each grid point, we record the predictive mean and the associated 95% prediction interval produced by the model. For TabPFN, the 95% prediction interval is obtained from the empirical 2.5% and 97.5% quantiles of the posterior predictive distribution. The coverage ratio is computed as the proportion of test points whose true function values fall within the predicted intervals, averaged over all repetitions. Similarly, the interval length is computed as the mean width of the predictive intervals, also averaged across all test points and repetitions. This evaluation jointly examines the calibration (via coverage ratio) and sharpness (via interval length) of the uncertainty estimates provided by TabPFN and GPR in both interpolation and extrapolation settings. The average coverage ratios and interval lengths for interpolation and extrapolation are reported in Table 9 and Table 10, respectively.

**Interpolation performance** (Table 9). In the interpolation region ( $x \in [-1, 1]$ ), TabPFN consistently exhibits coverage at around the nominal 95% level across all function types, indicating that it remains well-calibrated within the training distribution. In contrast, GPR fails to achieve the desired coverage under the step function, suggesting difficulty in handling discontinuities. Regarding interval length, TabPFN generally produces wider intervals than GPR when  $n = 11$ , particularly for nonlinear functions such as the quadratic and piecewise-linear cases, implying more conservative uncertainty estimates with limited data. As the training sample size increases to  $n = 31$ , TabPFN's intervals become narrower and comparable to those of GPR, reflecting sharper and still well-calibrated uncertainty estimates as data availability improves.

**Extrapolation performance** (Table 10). In contrast, the extrapolation region ( $x \notin [-1, 1]$ ) reveals a clear divergence between the two models. TabPFN maintains substantially higher coverage than GPR in nearly all cases. For smooth functions such as the linear and quadratic cases, GPR's coverage drops sharply (e.g., below 0.5 for the linear and below 0.1 for the quadratic function), indicating severe overconfidence

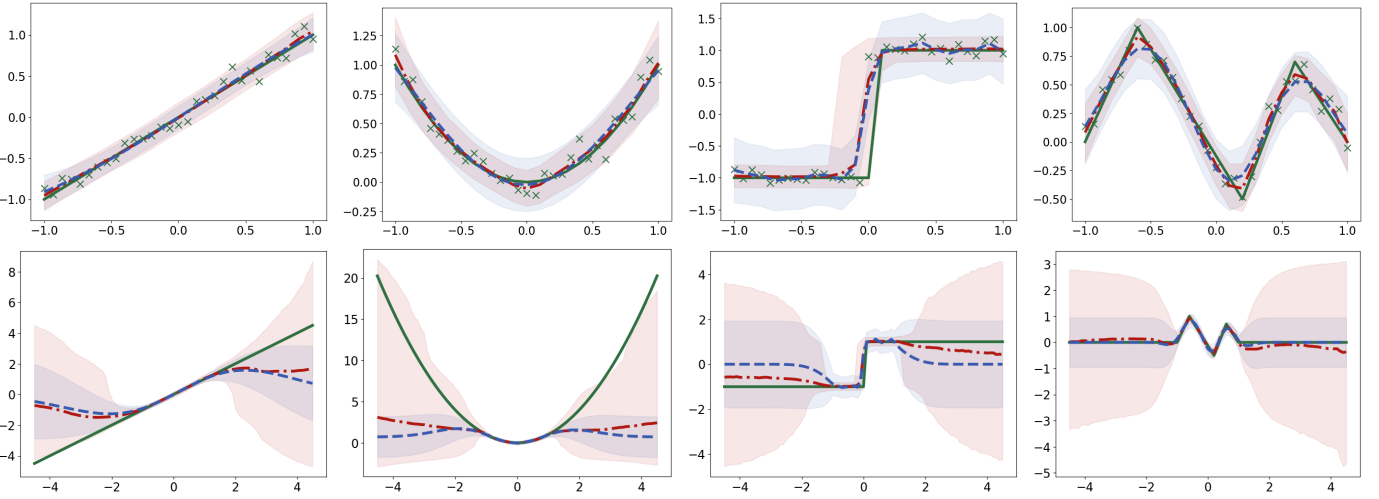


Fig 16: Interpolation (top) and extrapolation (bottom) performance of TabPFN (red) and Gaussian process regression (GPR; blue) regression on synthetic 1D functions, compared to ground truth (green). Columns correspond to different true functions: (i) linear, (ii) quadratic, (iii) step, and (iv) piecewise-linear. TabPFN shows the predicted mean (dash dotted line) with 95% prediction intervals (2.5%–97.5% quantiles; shaded region), while GPR displays the mean  $\pm$  1.96 SD (dashed lines). SD is the standard-deviation of the predictive distribution.

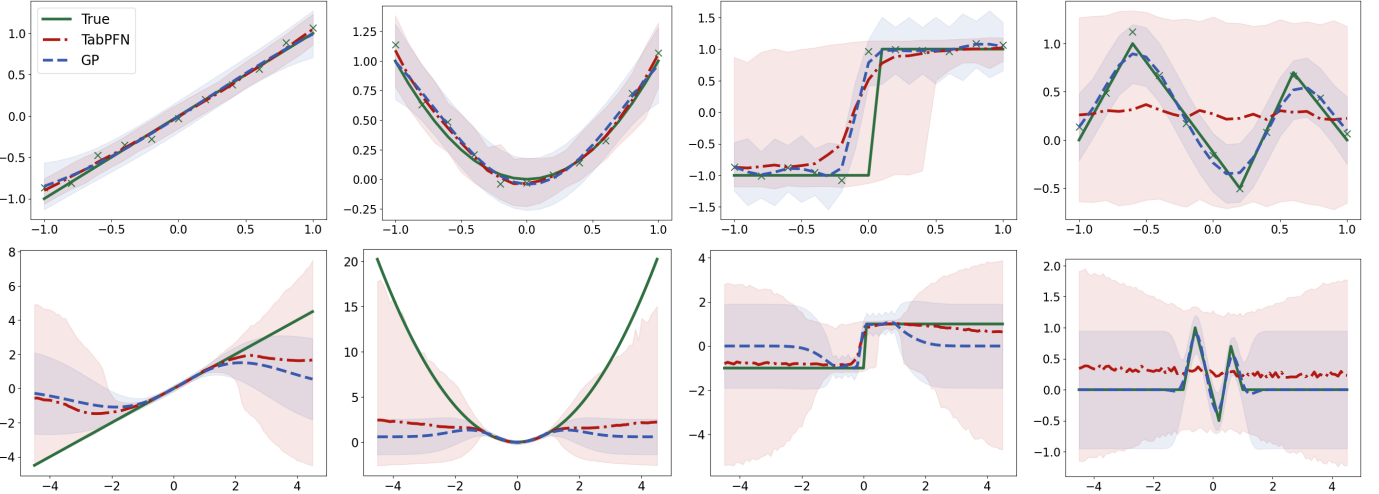


Fig 17: Interpolation (top) and extrapolation (bottom) performance of TabPFN (red) and Gaussian process regression (GPR; blue) regression on synthetic 1D functions, compared to ground truth (green) when  $n = 11$ . Columns correspond to different true functions: (i) linear, (ii) quadratic, (iii) step, and (iv) piecewise-linear. TabPFN shows the predicted mean (dash dotted line) with 95% prediction intervals (2.5%–97.5% quantiles; shaded red region), while GPR displays the mean  $\pm$  1.96 SD (shaded blue region). SD is the standard-deviation of the predictive distribution.

and poor uncertainty calibration outside the training range. TabPFN, however, achieves much higher coverage (0.93–0.98 for linear; 0.43–0.68 for quadratic) and adapts its interval width dynamically to reflect function complexity—producing wider intervals in regions of greater uncertainty (e.g., the quadratic case). For discontinuous or piecewise functions (step and piecewise-linear), both models attain full coverage, though TabPFN generally yields slightly longer in-

tervals, implying a more conservative but robust uncertainty quantification. Overall, TabPFN exhibits markedly better-calibrated uncertainty estimates than GPR under extrapolation, effectively avoiding the overconfident predictions that GPR commonly produces outside its training support.

**Summary.** These results demonstrate that while TabPFN and GPR perform comparably under interpolation, TabPFN provides superior extrapolative uncer-

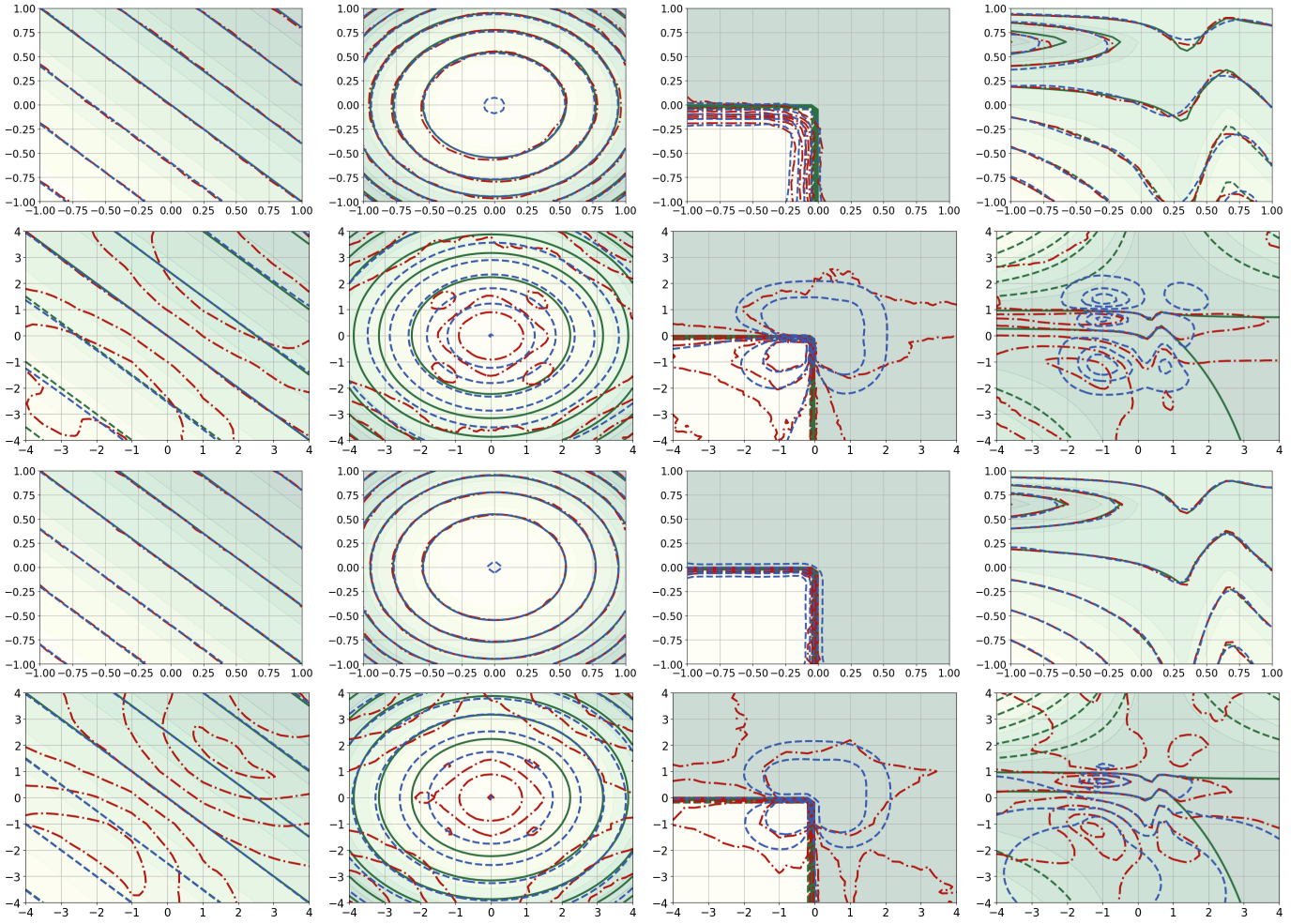


Fig 18: Performance comparison of TabPFN (red) and Gaussian Process (GP; blue) regression on synthetic 2D functions, evaluated against ground truth (green) using contour plots. Columns represent different true functions: (i) linear, (ii) quadratic, (iii) step, and (iv) piecewise-linear. Rows 1 & 2: Interpolation and extrapolation performance with a training set size of  $n = 11^2$ . Rows 3 & 4: Interpolation and extrapolation performance with a larger training set  $n = 31^2$ .

TABLE 9

*Average coverage ratio and interval length of TabPFN and Gaussian process regression (GPR) under the interpolation setting ( $x \in [-1, 1]$ ), averaged over 100 repetitions.*

n	Method	Linear		Quadratic		Step		P Linear	
		Coverage	Length	Coverage	Length	Coverage	Length	Coverage	Length
11	TabPFN	0.9350	0.4656	0.9525	0.7365	0.9705	1.2301	0.9930	1.8449
	GPR	0.9455	0.4304	0.9665	0.5439	0.8635	0.6934	0.9795	0.6977
31	TabPFN	0.9405	0.3924	0.9420	0.4235	0.9365	0.5501	0.9375	0.4788
	GPR	0.8775	0.3268	0.9390	0.4247	0.9050	0.5808	0.9550	0.5268

tainty quantification, maintaining both coverage and adaptive interval width even in regions far from the training data.

## APPENDIX E: SPARSE LINEAR REGRESSION

### E.1 Hyper-parameter selection

The LASSO and Ridge regression models are implemented using the *Lasso* and *Ridge* functions in the **scikit-learn** package, while the MCP and SCAD estimators are implemented using the **pycasso** pack-

TABLE 10

Average coverage ratio and interval length of TabPFN and Gaussian process regression (GPR) under the extrapolation setting ( $x \notin [-1, 1]$ ), averaged over 100 repetitions.

n	Method	Linear		Quadratic		Step		P Linear	
		Coverage	Length	Coverage	Length	Coverage	Length	Coverage	Length
11	TabPFN	0.9276	5.1478	0.4287	8.4742	0.9996	3.3699	1.0000	2.4744
	GPR	0.4856	2.9333	0.0792	2.7310	0.9997	2.4065	1.0000	1.7769
31	TabPFN	0.9827	5.9242	0.6817	11.9492	0.9975	3.8227	0.9993	4.9580
	GPR	0.6175	2.6130	0.0882	3.2259	0.9999	2.4096	1.0000	1.7710

age in Python. All four methods involve a regularization hyperparameter controlling the strength of penalization. For each method, we evaluate 20 candidate values of the tuning parameter and select the optimal one based on the prediction error computed on an independent validation set of size 1000. For LASSO, the regularization grid is chosen over the interval  $[0.001\|X_{\text{train}}^\top y_{\text{train}}\|_\infty, \|X_{\text{train}}^\top y_{\text{train}}\|_\infty]$ . For Ridge, SCAD, and MCP, the tuning parameter grids are respectively defined as  $[0.01, 100]$ ,  $[3, 100]$ , and  $[1.1, 100]$ . All grids are generated on a logarithmic scale with 20 evenly spaced points within the corresponding intervals.

## E.2 Additional results for sparse linear regression

The results under non-orthogonal design with beta-type 1 and beta-type 2 are given respectively in Figure 19 and Figure 20.

## E.3 ALE plot for TabPFN

The ALE plots of TabPFN under sparse linear regression are given in this section in Figure 21.

## APPENDIX F: IMPLEMENTATION DETAILS FOR LDA AND KNN

When  $X|Y=0 \sim \mathcal{N}(\mu_0, \Sigma)$  and  $X|Y=1 \sim \mathcal{N}(\mu_1, \Sigma)$ , with  $\pi = \mathbb{P}(Y=1)$ , the optimal Bayes classifier takes the form:

$$C^{\text{Bayes}}(x) = \begin{cases} 1, & \log\left(\frac{\pi}{1-\pi}\right) + \left(x - \frac{\mu_0 + \mu_1}{2}\right)^\top \Sigma^{-1}(\mu_1 - \mu_0) \geq 0, \\ 0, & \text{otherwise.} \end{cases}$$

The LDA classifier replaces population parameters with their sample estimates. Letting  $\tilde{Y}_i = Y_i$  for clean training data, we compute:

$$\begin{aligned} \hat{\pi} &= \frac{1}{n} \sum_{i=1}^n \mathbb{1}(\tilde{Y}_i = 1), \\ \hat{\mu}_r &= \frac{\sum_{i=1}^n X_i \mathbb{1}(\tilde{Y}_i = r)}{\sum_{i=1}^n \mathbb{1}(\tilde{Y}_i = r)}, \quad r \in \{0, 1\} \\ \hat{\Sigma} &= \frac{1}{n-2} \sum_{i=1}^n \sum_{r=0}^1 (X_i - \hat{\mu}_r)(X_i - \hat{\mu}_r)^\top, \end{aligned}$$

yielding the LDA classifier:

$$C^{\text{LDA}}(x) = \begin{cases} 1, & \log\left(\frac{\hat{\pi}}{1-\hat{\pi}}\right) + \left(x - \frac{\hat{\mu}_0 + \hat{\mu}_1}{2}\right)^\top \hat{\Sigma}^{-1}(\hat{\mu}_1 - \hat{\mu}_0) \geq 0, \\ 0, & \text{otherwise.} \end{cases}$$

For  $k$ -nearest neighbors ( $k$ NN) classification, we select the optimal number of neighbors  $k$  via 5-fold cross-validation. The search grid consists of 10 equally spaced integers between  $\lfloor n^{1/4} \rfloor$  and  $\lfloor n^{3/4} \rfloor$ , with the value maximizing cross-validation accuracy chosen for each experimental replication.

## FUNDING

Qiong Zhang is supported by the National Key R&D Program of China Grant 2024YFA1015800 and National Natural Science Foundation of China Grant 12301391. Yan Shuo Tan is supported by NUS Start-up Grant A-8000448-00-00 and MOE AcRF Tier 1 Grant A-8002498-00-00. Qinglong Tian and Pengfei Li are supported by the Natural Sciences and Engineering Research Council of Canada (RGPIN-2023-03479 and RGPIN-2020-04964).

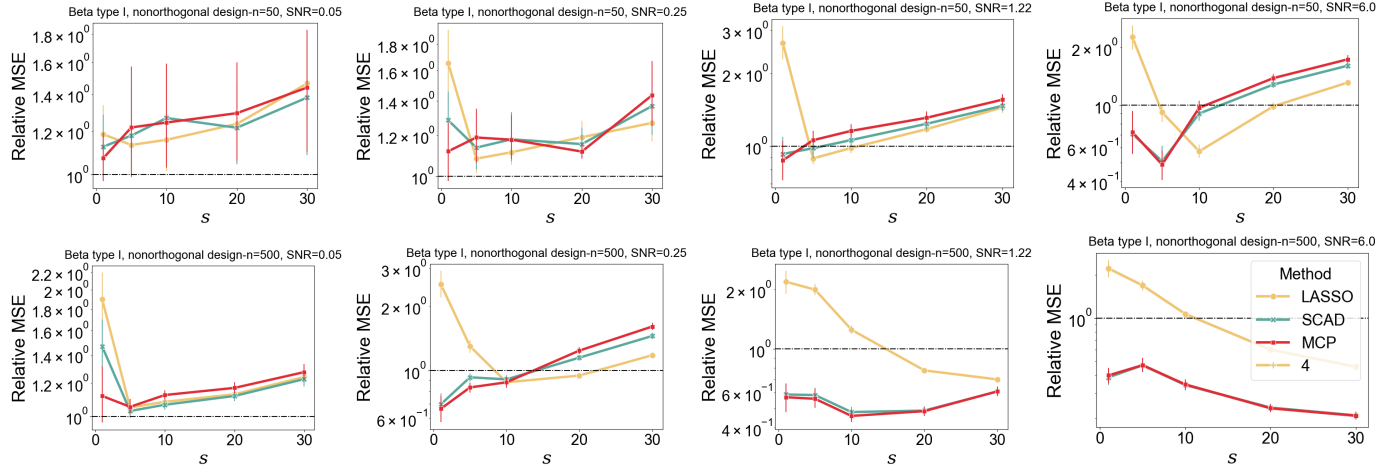


Fig 19: Relative test MSE of various methods compared to TabPFN. Experiments use beta-type 1 with nonorthogonal design. The top and bottom rows display results for  $n = 50$  and  $n = 500$  respectively, while the columns (from left to right) correspond to increasing SNR values.

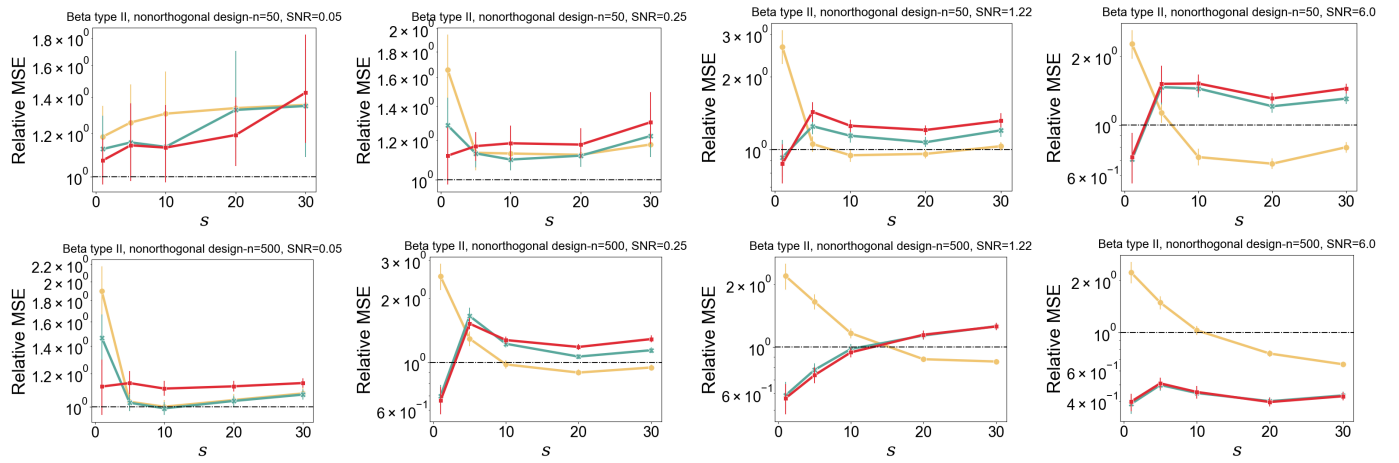


Fig 20: Relative test MSE of various methods compared to TabPFN. Experiments use beta-type 2 with nonorthogonal design. The top and bottom rows display results for  $n = 50$  and  $n = 500$  respectively, while the columns (from left to right) correspond to increasing SNR values.

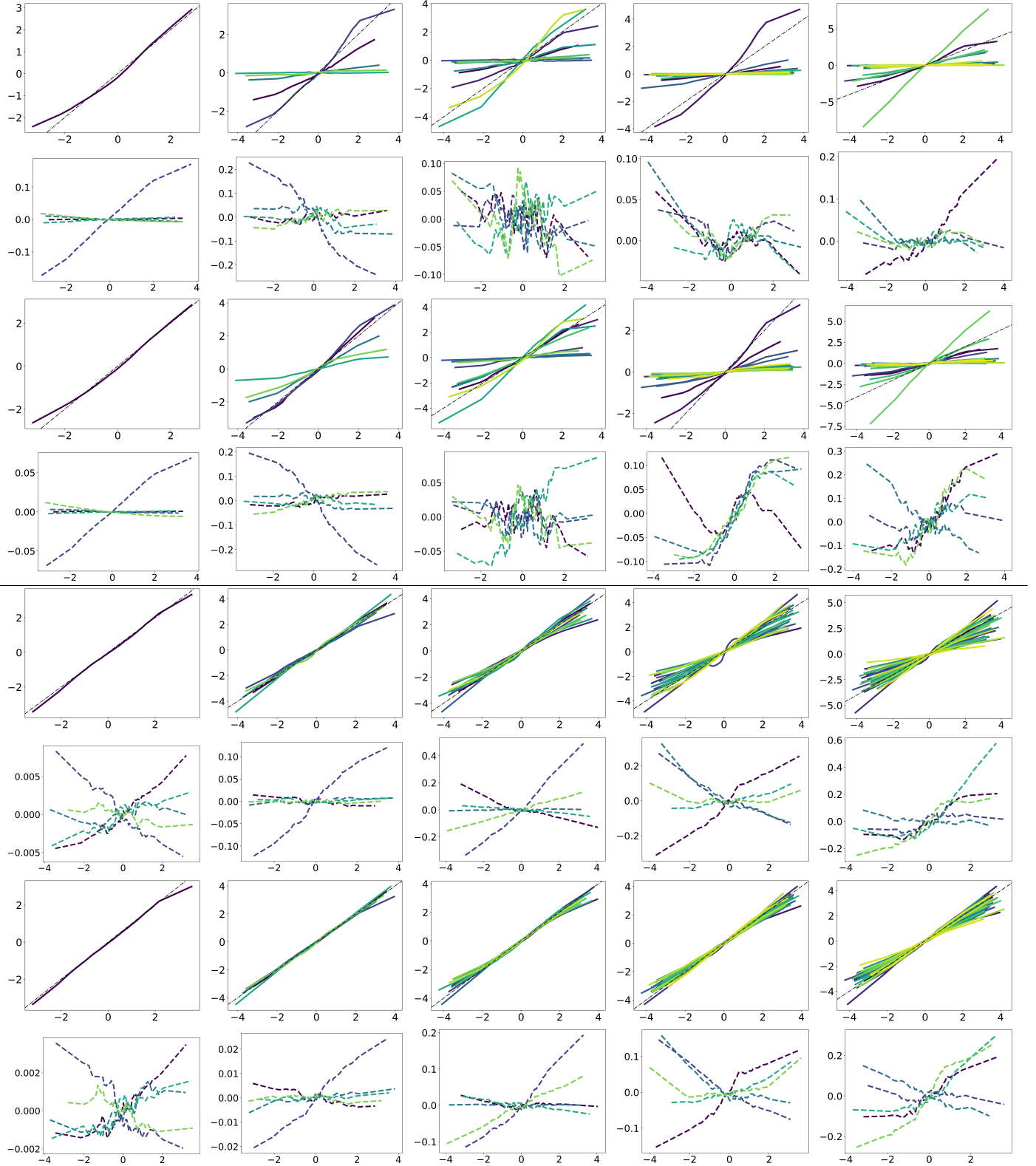


Fig 21: Accumulated Local Effects plot for TabPFN under sparse linear regression when  $d = 100$  under orthogonal design. Columns (left to right) correspond to increasing sparsity levels (1, 5, 10, 20, 30). Rows 1–4 show results when training set is of size  $n = 50$ . First row: Relevant feature; second row: randomly sampled 5 irrelevant features (SNR = 1.22). Third row: Relevant feature; fourth row: randomly sampled 5 irrelevant features (SNR = 6). Rows 5–8 show the same results when training set is of size  $n = 500$ .